

Magmatic signature of the closure of the northern branch of the Neo-Tethys: Upper Paleocene-Middle Eocene magmatism at the boundary of the Tavşanlı-Sakarya Zone (Turkey)

Bahattin GÜLLÜ^{1,*} and Yusuf Kağan KADIOĞLU^{2,3}

- 1 Aksaray University, Faculty of Engineering Department of Geological Engineering, Aksaray, Turkey
- 2 Ankara University, Earth Sciences Application and Research Centre (YEBİM), Ankara, Turkey
- 3 Ankara University, Faculty of Engineering Department of Geological Engineering, Ankara, Turkey



Güllü, B., Kadioğlu, Y.K., 2022. Magmatic signature of the closure of the northern branch of the Neo-Tethys: Upper Paleocene-Middle Eocene magmatism at the boundary of the Tavşanlı-Sakarya Zone (Turkey). *Geological Quarterly*, 2022, 66: 13, doi: 10.7306/gq.1645

Associate Editor: Lilit Sahakyan

Numerous plutons composed of granite, granodiorite, diorite-porphyr, monzonite, granodiorite-porphyr and diorite/microdiorite-porphyr occur at the boundary of the Tavşanlı-Sakarya Zone, in the eastern part of the northwestern Anatolian magmatic belt, Turkey. These rocks belong to two different types: a medium-K calc-alkaline granodiorite series (with associated dykes and sub-volcanic rocks) and a shoshonitic series of granites. The rocks of the shoshonitic series have SiO₂ from 67.5 to 75.6 wt.% with Mg# from 35.1 to 59.5, whereas the medium-K calc-alkaline series rocks have SiO₂ between 54.6 and 67.7 wt.% with Mg# from 43.5 to 60.8. There is a clear enrichment of LILE with respect to the HFSE in all magmatic units of the region. These magmatic rocks reflect properties of collision-related arc magmatism in the various geochemical discrimination diagrams. The initial ⁸⁷Sr/⁸⁶Sr and ¹⁴³Nd/¹⁴⁴Nd isotopic ratios of the magmatic units range from 0.705506 to 0.710902 and 0.512178 to 0.512594, respectively. Collision-related granitoids yielded a ⁴⁰Ar/³⁹Ar cooling age age of 59.13 ± 1.87 Ma, and arc-related granitoids and associated sub-volcanic units 44.3 ± 0.47 and 44.11 ± 0.89 Ma. The data obtained revealed that continent-continent collision in the Paleocene together with the initiation of the closure of the Neo-Tethys took place between the Anatolide-Tauride Platform and Sakarya Plate from the end of the Cretaceous. The shoshonitic granite may cooled in the Middle Paleocene, as regards the subduction-accretion zone in which subduction impacts have been observed. The medium-K calc-alkaline magmatic products in the region were formed by partial melting of the continental lithospheric mantle caused by the upwelling of asthenospheric mantle after the subducted slab was delaminated.

Key words: cooling age, sub-volcanic phase, shoshonites, enclave, petrological modelling.

INTRODUCTION

The closure of the Tethys Ocean is represented by two main suture zones in Turkey: the İzmir-Ankara-Erzincan and Intra Pontid suture zones. Both suture zones were formed during continental collisions following the northwards subduction of the Tethys oceanic lithosphere. In addition, the closure of the Tethys Ocean occurred in two intervals in Turkey: the Carboniferous-Triassic (Palaeo-Tethys) closure and the Triassic-Cretaceous (Neo-Tethys) closure (Okay and Tüysüz, 1999).

The closure of the Neo-Tethys, which played an important role in shaping the microcontinents and platforms of Anatolia,

started in the Triassic-Cretaceous and continued until the continental collision in the Paleocene-Early Eocene (Altunkaynak and Dilek, 2013). The magmatic belt along the İzmir-Ankara-Erzincan Suture Zone is represented by intrusive, sub-volcanic and related volcanic rocks (Keskin et al., 2008; Dilek and Altunkaynak, 2009; Karlı et al., 2010; Kaygusuz et al., 2011; Eyuboglu et al., 2011; Altunkaynak and Dilek, 2013; Aysal et al., 2018; Özyurt and Altunkaynak, 2020). In previous studies, which included limited radiometric data, it was generally accepted that the magmatic rocks in the region related to the post-collisional setting formed during the Late Paleocene-Early Eocene (Harris et al., 1994; Altunkaynak and Dilek, 2006; Dilek and Altunkaynak, 2009). These magmatic rocks, which shed light on Turkey's geodynamic evolution, have been variously investigated (Güleç, 1991; Genç, 1998; Aldanmaz et al., 2000; Okay, 2002; Aydoğan et al., 2008; Dilek and Altunkaynak, 2009; İlbeyli and Kibici, 2009; Zoroğlu, 2009; Altunkaynak et al., 2012a, b; Güllü, 2012).

* Corresponding author, e-mail: bgullu@aksaray.edu.tr

Received: September 2, 2021; accepted: April 5, 2022; first published online: August 22, 2022.

The granitoids located at the boundary of the Tavşanlı-Sakarya Zone are the first products of Paleogene magmatism in northwestern Anatolia. These granitoids are significant to the interpretation of the consequences for closure of the northern branch of the Neo-Tethys, which shaped the geodynamic structure of the region. There are three main models for the genesis of the magmatic bodies in the region. The first and widely accepted model is that these magmatic bodies are associated with the northwards subduction of the Neo-Tethys under the Sakarya microcontinent (Altunkaynak, 2007; Karacik et al., 2008). The second model is collision-driven via slab break-off (Altunkaynak et al., 2012a; Demirbilek et al., 2018). The third and less widely accepted model is that these magmatic bodies are derived from the subduction of Neo-Tethys under the Tauride-Anatolide Platform (Bağcı et al., 2019). There are different opinions regarding the subduction direction. Previous studies on the regional geology propose that the neo-Tethys was consumed by subduction under the Sakarya continent. This paper examines the controversial geodynamics of the magmatic rocks in the region together with the isotopic and radiometric data of the Karakaya, Topkaya and Yürükkaracaören magmatic units. The Topkaya and Yürükkaracaören magmatic units have not been considered in previous studies. Also, the original relationship between the Yürükkaracaören sub-volcanic rocks and the Topkaya magmatic units, which were classified as “granodiorite” in previous studies, has been revealed for the first time in this study with radiometric, isotopic and extensive geochemical data. In addition, the comparative petrogenetic relations of the magmatic bodies formed by the differentiation of the magma forming the intrusive rocks in the region are also discussed in detail for the first time.

GEOLOGICAL SETTING

Northwestern Anatolia consists of many micro-blocks involved in the continent-continent collision following the closure of the Tethys Ocean by northwards subduction (Şengör and Yılmaz, 1981; Okay and Tüysüz, 1999). The basement of northwestern Anatolia consists of Permian metamorphic rocks (Altınlı, 1973; Yılmaz, 1981; Okay, 1984a). Apart from these, there are three main metamorphic belts consisting of the Mesozoic Karakaya complex and the Tavşanlı and Afyon zones in the northwestern Anatolia (Okay, 1984a, b; Fig. 1A).

The Karakaya complex represents an accretionary prism which originated as a result of subduction of the Paleotethys in the Triassic towards the north along the active margin of Laurasia (Okay and Gönçüoğlu, 2004). The complex underwent metamorphism at greenschist facies in the Triassic (Okay, 1984b).

The Tavşanlı Zone is represented by Cretaceous high pressure/low-temperature metamorphic rocks derived from the northern section of the Anatolide-Tauride Block (Okay, 1984a, b; 2011). Okay (1984a, b) stated that the units forming the Tavşanlı Zone consist of ophiolitic melanges and Eocene sedimentary and the intrusive units. The units of the Tavşanlı Zone in the Ordovician metagranitic basement are considered to be a tectonic slice (Okay et al., 2008). The crystallization age of the intrusive unit is 467.0 ± 4.5 Ma based on U/Pb single zircon evaporation analyses. These Ordovician rocks are inferred to have originated during rifting and separation of small plates such as the Istanbul Plate from the northern margin of Gondwana (Okay et al., 2008). While the thick sedimentary units of the Tavşanlı Zone have been obducted onto the Afyon Zone. The Afyon Zone has undergone low-grade regional metamor-

phism, and consists of Permo-Carboniferous clastic, Triassic-Campanian platform carbonate and Maastrichtian pelagic strata. Ophiolite nappes lie on top of it (Okay, 1984a, b).

The oldest unit in the study area is formed by the metamorphic Sivrihisar Massif having a similar protolith to the rest of the Tavşanlı Zone (Whitney et al., 2011). The greenschist facies rocks at the bottom and the marbles at the top form the dominant lithologies among the Sivrihisar metamorphic rocks. The marbles forming the upper levels of the metamorphic units have tectonic contacts with the Karakaya (Kaymaz) granites.

This study covers the magmatic bodies located in the easternmost part of the northwestern Anatolian magmatic belt, at the boundary between the Sakarya microcontinent and the Tavşanlı Zone (Fig. 1A). The first geochronological study regarding the emplacement and cooling ages of the magmatic suites under discussion was by Gautier (1984), who made a U-Pb radiometric analysis of zircons and apatites in the pluton, obtaining ages of 84.98 ± 6.27 and 65.91 ± 3.84 Ma for two magmatic units. Shin et al. (2013) found that crystallization of the Sivrihisar and Kaymaz granitoids occurred during the Eocene, following subduction in the Early-Late Cretaceous. Demirbilek et al. (2018) stated that the Karakaya (Kaymaz) granite originated at 52.1 ± 2.0 and 54.0 ± 2.1 Ma from K-Ar dating.

SAMPLING AREA

The field observations were made of three intrusive units (Fig. 1B–D). The Karakaya (Kaymaz) granite is located in the south-west of the study area. It covers an area of 16 km², and has a very hilly topography. In the pluton, regular jointing has been observed; while fresh surfaces are pale grey, subaerial surfaces undergoing weathering are yellowish-grey (Fig. 2A).

The Karakaya granite is cut by aplitic dykes ranging from 1 cm up to 2 m thick, with tectonic trends N 30°W to N 60°W. Tourmaline-bearing quartz veins up to 20 cm thick have also been observed in the pluton. Quartz, plagioclase, alkali feldspar, biotite, tourmaline and rarely reach up to 15 cm across were observed within the main unit, mainly composed of quartz, plagioclase, hornblende and biotite (Fig. 2C).

The Topkaya granitoid crops out over an area of ~45 km² in the northwestern part of the study area. Light grey diorite porphyry and granodiorite varieties can be distinguished here. The pluton shows a diorite porphyry composition with porphyrophanitic texture as a marginal facies, and granodiorite with phaneritic texture developed towards the central part (Fig. 2D). Mafic microgranular enclaves from 1 to 25 cm in size are mostly distributed at the margins of the pluton. These ellipsoidal-spheroidal enclaves could be easily distinguished from the Topkaya granitoid due to their darker colour and finer-grained texture (Fig. 2E). Also, there are some zones with needle-shaped mafic minerals within felsic minerals, 10–20 cm across, in the granodiorites. These zones, termed appanite (Fig. 2F), were interpreted by Sha (1995) as a result of local mixing of mafic and felsic magmas. The Topkaya granitoid is cut by felsic and intermediate veins. The intermediate veins range in width from 1 cm to 2 m and are up to several hundred metres in length. These rocks have porphyritic textures and have the composition of microgabbro porphyry, microdiorite porphyry, diorite porphyry and granodiorite porphyry.

There are Yürükkaracaören sub-volcanic units, originally related to the Topkaya granitoid, in the northeastern part of the study area. Sub-volcanites show porphyritic texture and consist of biotite, amphibole and feldspar (Fig. 2G). Quartz-hornblende ocellar texture and magmatic segregation enclaves are macro-

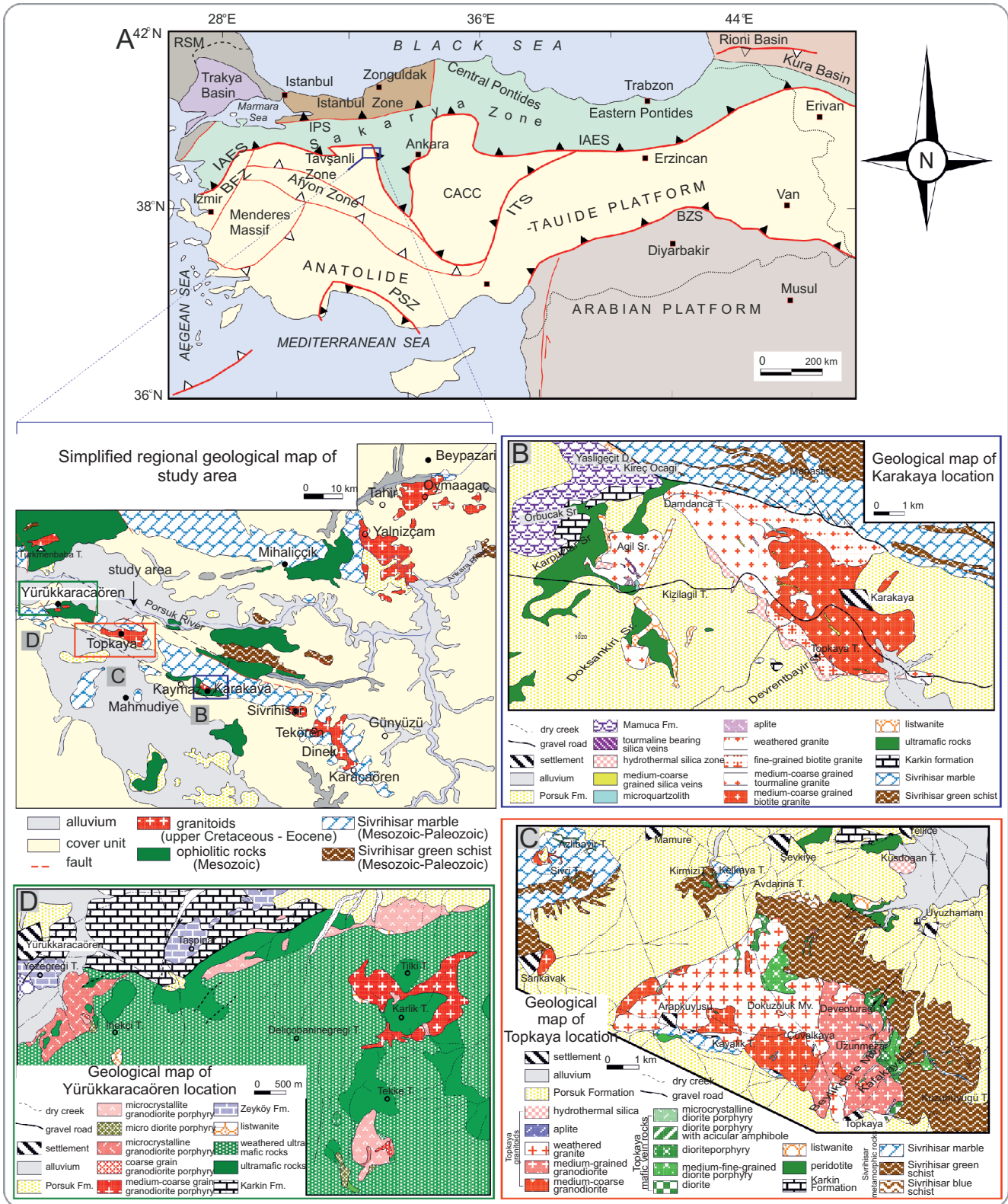


Fig. 1A – location of the study area with respect to the tectonic units of Turkey (simplified from Okay, 2011) and magmatic facies maps of the rocks located in the (B) Karakaya, (C) Topkaya and (D) Yürükkaracaören areas

BFZ – Bornova Flysch Zone, BZS – Bitlis-Zagros Suture, CACC – Central Anatolian Crystalline Complex, IAES – İzmir-Ankara-Erzincan Suture, ITS – Inner Tauride Suture, PSZ – Pamfilia Suture, RSM – Rhodope-Strandja Massif

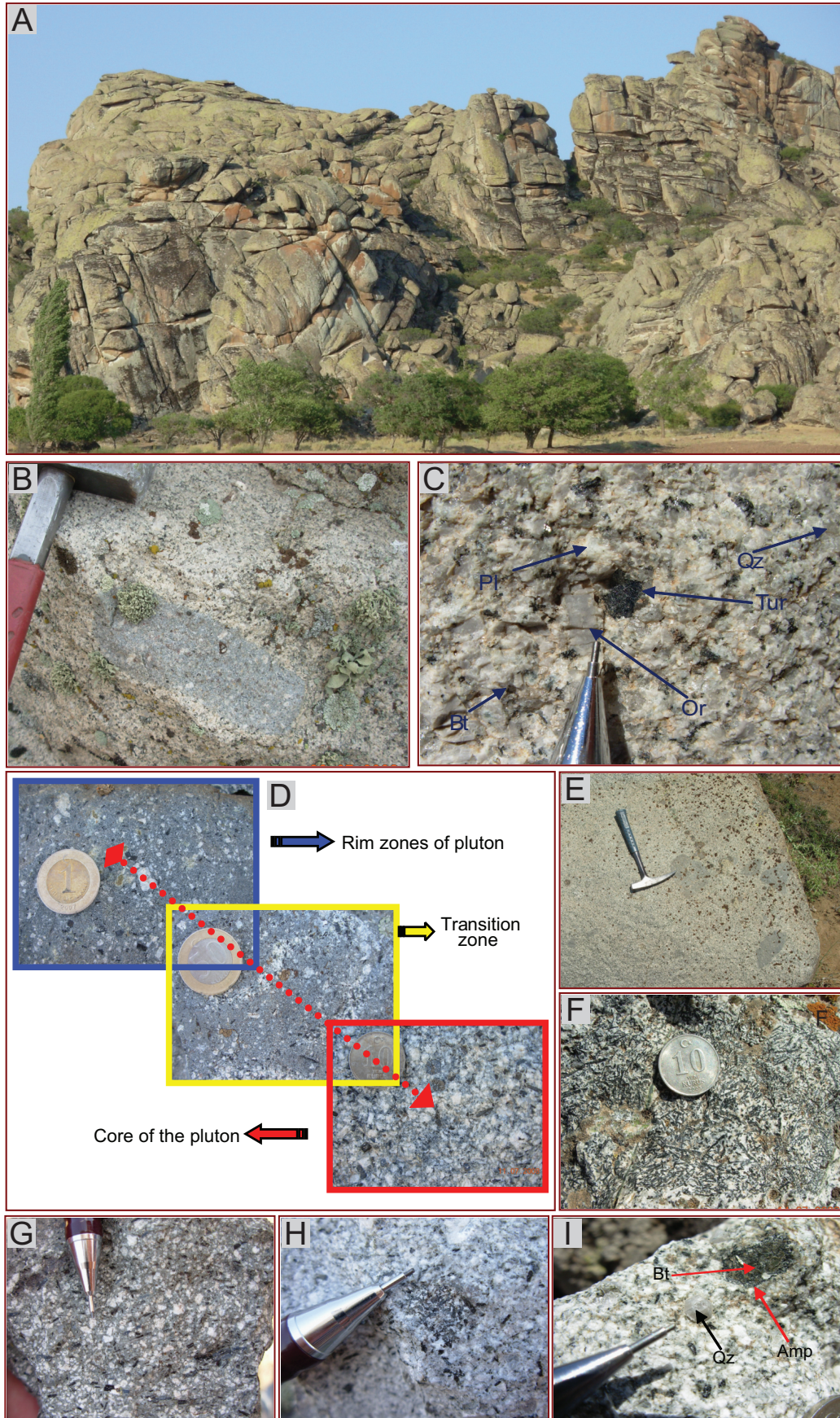


Fig. 2A – view of the Karakaya granite; **B** – enclaves within the granites; **C** – close-up view of the Karakaya granite; **D** – mineralogical and textural changes of the Topkaya pluton from rim to core; **E** – mafic microgranular enclaves within the granodiorites; **F** – apatite-type enclaves within the granodiorites as local units; **G** – macroscopic view of diorite porphyry; **H** – mafic magmatic enclave within Yürükkaracaören diorite porphyries; **I** – euhedral quartz and magmatic segregation enclave in diorite porphyry

Amp – amphibole, Bt – biotite, Or – orthoclase, Pl – plagioclase, Qz – quartz, Tur – tourmaline

scopically observed in the host rock (Fig. 2H). Biotite, amphibole and secondary quartz are seen in the rock (Fig. 2I).

Sub-volcanitic rocks, considered to be originally related to the Topkaya pluton, may represent the upper levels of a pluton.

The magmatic units are unconformably overlain by Neogene-Quaternary strata. Magmatic facies maps of all three locations have been prepared based on the textural properties and petrographic characteristics of the magmatic rocks as observed in the field (Fig. 1B–D).

ANALYTICAL TECHNIQUES

Petrographic analyzes were carried out in the petrographic research laboratory of the Ankara University Earth Sciences Application and Research Center using a *Leica DM 2500P* polarizing research microscope.

The geochemical analyses were conducted in the Earth Science Application and Research Center Laboratory (YEBİM) of Ankara University. The chemical composition of the samples was determined using a *Spectro XLAB 2000 Polarized Energy Dispersive X-Ray Fluoresans* (PEDXRF) device. The analytical results were calibrated using the *GEO-7220*, *K02-GSR-09* and *G01-GS-N-Granite USGS* standards. The samples were finely grounded in a ball mill to a dimension of 20 microns. Afterwards, a 4 g sample was mixed with 0.9 gr wax and compressed with a press at 15×10^4 N/m².

Trace element analyses were made by ICP-MS in the Bureau Veritas Mineral Laboratories (Canada), using the *SO-18* standard according to USGS standards and with calibration of the device. For ICP-MS, the samples were calcined and dissolved in appropriate acids in preparation for analysis.

Sr and Nd isotope analysis was performed in the METU Central Lab R&D Training and Measurement Center Radiogenic Isotope Lab. The Sr was separated with 2.5 N HCl acid using *Bio Rad AG50 W-X8*, 100-200 mesh resin with 2 mL volume. After the collection of strontium, 6 N HCl was used and the rare earth element fraction was collected. Strontium was loaded onto single Re-filaments using a Ta-activator. ⁸⁷Sr/⁸⁶Sr data were normalized to ⁸⁶Sr/⁸⁸Sr = 0.1194. During the measurements, a Sr NBS 987 standard was measured as 0.710260 ± 5 (n = 2) and necessary corrections were made to the measurement results. Neodymium was separated from other rare earth elements by passing over 2 mL volume HDEHP (bis-ethoxyethyl phosphate) covered biobeads acid by using 0.022 N HCl. The separated neodymium was loaded onto a filament together with 0.005 N H₃PO₄. During the analyses; ¹⁴³Nd/¹⁴⁴Nd data were normalized with ¹⁴⁶Nd/¹⁴⁴Nd = 0.7219 and the Nd LaJolla standard was measured as 0.511850 ± 5 (n = 2). ¹⁴³Nd/¹⁴⁴Nd and ⁸⁷Sr/⁸⁶Sr ratios, initial ⁸⁷Sr/⁸⁶Sr ratios of the rock groups and εNd values were calculated according to Ar-Ar age analysis results.

Ar-Ar age analysis was made on biotite minerals with a *Finnigan MAT-262 Thermal Ionisation Mass Spectrometry* (TIMS) device in the Institute of Geology and Geophysics, Chinese Academy of Sciences, Radiogenic Isotope Geochemistry Laboratories. The mineral selection for Ar-Ar analysis was made manually from crushed rock samples. The selected samples were then irradiated to produce ³⁹Ar from ³⁹K. Heating causes the crystal structure of the mineral (or minerals) to degrade, and, as the sample melts, trapped gases are released. All the measurements were performed by mass spectroscopy.

RESULTS

PETROLOGY

During the crystallization of magma, many groups of igneous rock can form by differentiation. The original relationships, mineralogical compositions and textural properties of these rock groups, forming different magmatic facies, can be revealed by petrological studies. More than 500 thin-sections of different varieties of granitoid rock were examined.

KARAKAYA (KAYMAZ) GRANITE

According to the IUGS classification, all magmatic rocks in Karakaya location are of granitic composition. In the magmatic facies distinction based on mineralogical composition, the magmatic products in the region were classified for the first time in this study as biotite granite and tourmaline biotite granite according to the dominant mineral composition. The Karakaya granite is cut by felsic vein rocks such as alkaline feldspar granite, granophyre and quartzolite.

Biotite granite; biotite granite mineralogically consists of quartz + orthoclase + plagioclase (An₁₁-An₁₅) + biotite ± titanite ± allanite ± zircon ± opaque mineral. In addition, sericite, chlorite, calcite and rarely epidote are observed as alteration products. Biotite granites generally possess holocrystalline hipidiomorph granular texture (Fig. 3A). Zircons are observed as inclusions in the biotites (Fig. 3B) and allanite (orthite) and titanite are seen as euhedral crystals (Fig. 3C).

Tourmaline-biotite granites; tourmaline-biotite granites have a similar mineral composition to the biotite granites and are characterized by a significant tourmaline content. The tourmalines are observed in myrmekitic-like textures in the shape of anhedral crystal forms (Fig. 3D). Güllü and Kadioğlu (2017) stated that these tourmalines are of schorl composition. Fluorite has been detected for the first time in this study within the tourmaline-biotite granites (Fig. 3E). The tourmaline-bearing granite may have been affected by metasomatic processes, and the presence of tourmaline distinguishes these granites from the non-metasomatic biotite granite.

Felsic vein rocks and hydrothermal products; aplites which alkali feldspar granite, granophyre and quartzolite in composition represent veins cutting host rock. Quartz + orthoclase + plagioclase + biotite + tourmaline are the main components of these aplites. These units, representing the late-stage products of the Karakaya granite, include varieties with and without tourmaline. Güllü and Kadioğlu (2012) stated that the tourmaline-bearing quartz veins may be the products of residual Na-depleted melts (Fig. 3F).

TOPKAYA GRANITOID

These rocks can be classified as granodiorite and quartz monzonite. The intermediate vein rocks are microdiorite, diorite porphyry and microcrystalline diorite porphyry in composition.

Granodiorite; granodiorite mainly consists of quartz + plagioclase (An₂₂-An₄₈) + orthoclase + hornblende + biotite ± titanite ± apatite ± zircon. Chlorite and epidote are alteration products (Fig. 3G). The granodiorite has holocrystalline

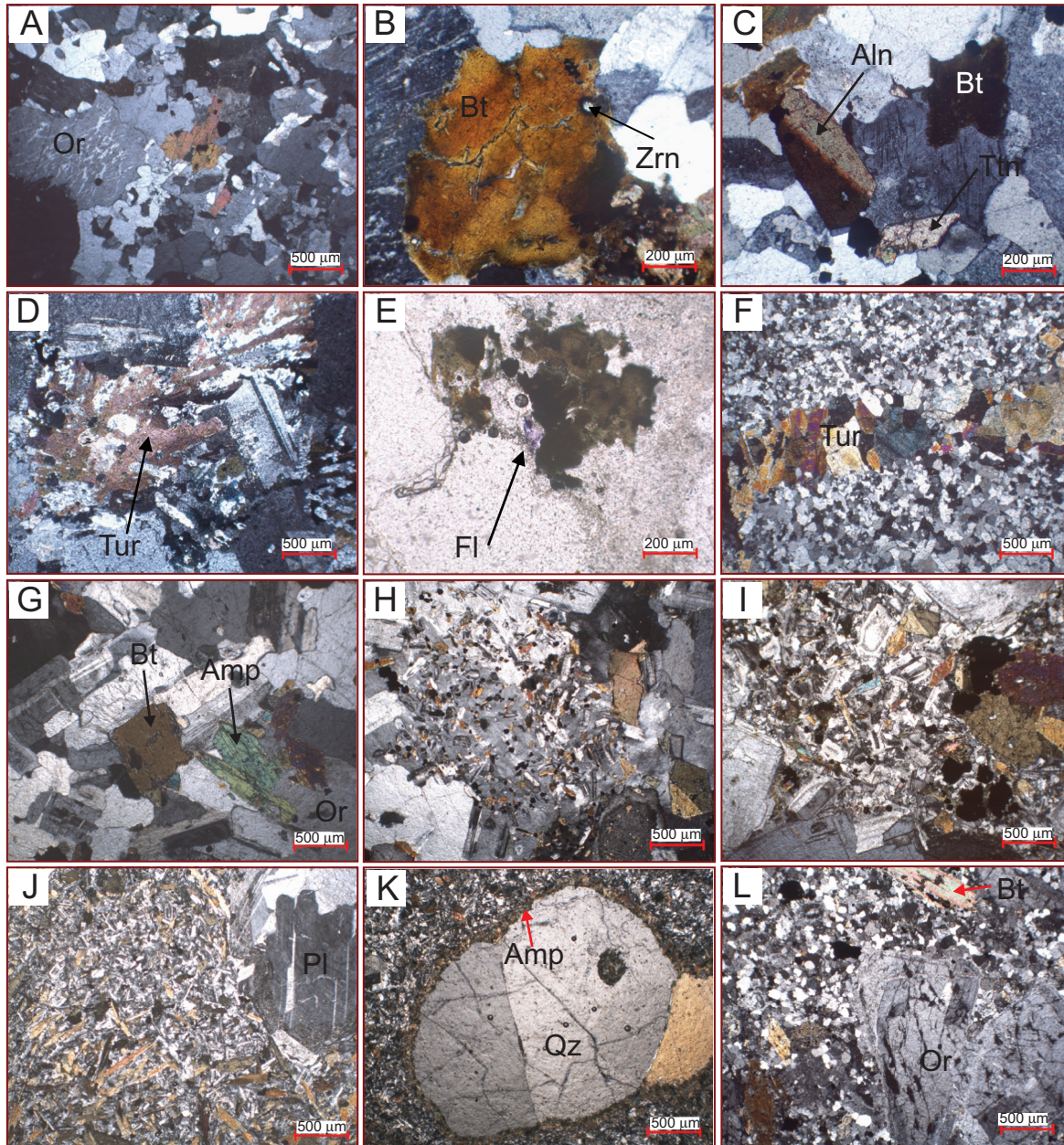


Fig. 3A – general microscopic view of the Karakaya granite; B – zircon (Zrn) inclusion within biotite (Bt) in granite; C – euhedral titanite (Ttn) and allanite (Aln) within granite; D – crossed-polars view of tourmaline (Tur) within tourmaline biotite granite under a polarizing microscope; E – fluorite (Fl) observed in tourmaline biotite granite; F – view of tourmaline-bearing silica vein under a polarizing microscope; G – general microscopic view of the Topkaya granitoid; H – poikilitic K-feldspar occurrences in the granitoid; I – general microscopic view of diorite porphyry; J – microphoto views of acicular amphibole microdiorite porphyries; K – quartz-hornblende ocellar texture occurrences in diorite porphyries; L – general microphoto views of Yürükkaracaören granodiorite porphyries (mineral abbreviations are according to [Whitney and Evans, 2010](#))

hipidiomorph granular texture (with features such as poikilitic K-feldspar, acicular apatite; [Fig. 3H](#)).

Intermediate vein rocks; the vein rocks have been classified as medium-coarse crystalline gabbro/diorite porphyry, fine-grained diorite porphyry, acicular amphibole microdiorite porphyry and microcrystalline granodiorite porphyry ([Fig. 3I, J](#)). In addition, the intermediate vein rocks have lath-shaped plagioclases and quartz-hornblende ocellar texture ([Fig. 3K](#)).

YÜRÜKKARACAÖREN SUB-VOLCANIC UNITS

This rock unit was previously termed “granodiorite” ([Gautier, 1984; Demirbilek et al., 2018](#)). However, a characteristic holocrystalline hypidiomorph porphyritic texture was observed in all samples collected from Yürükkaracaören. With the textural features of microcrystalline porphyry, the rocks of the Yürükkaracaören location show shallow-emplacment sub-vol-

canic rock characters. Therefore, these rocks are here described as sub-volcanic based on detailed field and petrographic features. This sub-volcanic unit is generally diorite porphyry and granodiorite porphyry in composition (Fig. 3L). The mineralogical composition is mainly plagioclase + orthoclase (in granodiorite porphyry) + quartz (in granodiorite porphyry) + biotite + hornblende ± opaque mineral ± titanite ± apatite.

WHOLE-ROCK GEOCHEMISTRY

One of the most characteristic features of granitoid bodies is magmatic differentiation and/or magma mixing during crystallization. In order to detect the presence of magmatic differentiation or magma mixing, a large number of geochemical analyses are required on systematically collected samples. Geochemical analysis was performed on 329 samples (Appendix 1) to constrain magmatic differentiation or magma mixing in these granitoid bodies and to map the magmatic facies.

MAJOR ELEMENT VARIATIONS

All units and enclaves within the Karakaya granite are granitic in composition according to the total alkali versus silica diagram (Cox et al., 1979; Fig. 4A). While SiO₂ content is in the range of 67.5–76.0% in the granitic rocks, it is within the range of 62.4–72.7% in enclaves. The enclaves of the Topkaya granitoid fall within the gabbro/diorite-diorite and rarely monzonite area on the same diagram. The main body of the Topkaya intrusion plots in the granodiorite field (Fig. 4A).

The aplite dykes that cut all the magmatic units in the Topkaya granitoid are of granitic composition. The intermediate vein rocks which are observed commonly in the granitoids range from gabbro/diorite to granodiorite. The Yürükkaracaören sub-volcanic units lie in the diorite and granodiorite fields on the total alkali-silica diagram (Fig. 4A). Na₂O wt.%, SiO₂ wt.%, and K₂O wt.% contents increase, whereas CaO wt.%, MnO wt.%, MgO wt.%, Fe₂O₃ wt.%, and TiO₂ wt.% decrease from microcrystalline diorite porphyries to microcrystalline granodiorite porphyries in the sub-volcanic rocks.

The Karakaya, Topkaya and Yürükkaracaören magmatic units lie in the sub-alkaline field on the Na₂O + K₂O (wt.%)–SiO₂ (wt.%) diagram (Irvine and Baragar, 1971; Fig. 4B). In addition, on the AFM diagram, while the Karakaya granite shows calc-alkaline character, the Topkaya granitoid and Yürükkaracaören sub-volcanic rocks show a trend from tholeiitic to calc-alkaline (Fig. 4C).

On the alumina saturation diagram (Maniar and Piccoli, 1989), based on the Shand (1943) indices, while the Topkaya granitoid and Yürükkaracaören sub-volcanic units show metaluminous character, the Karakaya granites are characteristic in showing a transition from peralkaline to metaluminous (Fig. 4D). The ACNK (where ACNK = molar Al₂O₃/CaO + Na₂O + K₂O) ratio of the granitoid samples ranges between 1.13 and 1.54 in the Karakaya granite, 1.17–1.63 in the Topkaya granitoid and 1.45–1.74 in the Yürükkaracaören sub-volcanic rocks.

The Karakaya granite shows K series character on a K₂O versus Na₂O diagram (Middlemost, 1975; Fig. 4E). In addition, shoshonitic character is dominant on a K₂O–SiO₂ diagram (Rickwood, 1989; Fig. 4F). The Topkaya granitoid and the Yürükkaracaören sub-volcanic rocks may be clearly distinguished from the Karakaya granite through their Na series and medium K calc-alkaline magma characters.

The granite and granodiorite/sub-volcanic rock units are regionally separated on discrimination diagrams of the major ele-

ments. According to these diagrams, the igneous rocks, including enclaves at the Karakaya location, differ chemically from the rocks from Topkaya and Yürükkaracaören (Fig. 5A–G).

On the Harker variation plots of SiO₂ versus major oxides by the rock units. Alkali (Na₂O + K₂O) content increases with SiO₂, whereas TiO₂, Fe₂O₃, CaO, Al₂O₃, MgO and in part P₂O₅ decrease as SiO₂ increases. As in the major element oxide changes, while a common trend has been observed in the Topkaya and Yürükkaracaören magmatic rocks on the trace element distribution diagrams, the Karakaya granite shows a different trend.

Sr, Ni, Zn and Y show a decreasing trend relative to increasing SiO₂ (Fig. 5H–K). This decrease could be expressed through the plagioclase fraction for Sr and expressed through the crystallization of accessory minerals for Zn and Y. Similarly, zircon crystallization may impoverish magma in Zr and this is evident from a SiO₂ versus Zr diagram (Fig. 5L). Th and Rb are notable as the final phase products of crystallization in all the magmatic units. The Karakaya granite contains higher concentrations of Th, Rb and Nb than do the other rock masses (Fig. 5M–O). The high concentrations of Th and Rb reflect the interaction of a shoshonitic granite with the continental crust. The high Nb concentrations in the Karakaya granite may represent enrichment during the transition from a magmatic to a pegmatitic phase (Ballouard et al., 2016; He et al., 2021). No significant change has been observed in the Hf concentrations (Fig. 5P). The linear trends in all major elements versus SiO₂ and trace elements versus SiO₂ indicate magma mixing (Slaby and Martin, 2008).

Temperature (T) during the crystallization of igneous rocks can be calculated with the help of empirical formulae recommended by different researchers (Harrison and Watson, 1984; Schmidt, 1992; Miller et al., 2003; Koralay et al., 2021 and references therein). Zircon and apatite saturation temperatures were calculated from whole-rock geochemical analyses according to Watson and Harrison (1983) and Harrison and Watson (1984). The chemical dependencies of apatite and zircon saturation temperatures are different. Apatite saturation depends on SiO₂ and P₂O₅ concentrations in magma. The zircon saturation depends on the M factor [(Na + K + 2 · Ca)/(Al · Si)]. Magma crystallization depth, pressure and H₂O content do not have a significant effect on zircon and apatite saturation temperature (Janasi et al., 2007). Temperatures from zircon saturation calculations are 740–793°C (~767°C) for the Karakaya granite, 716–763°C (~735°C) for the Topkaya granitoid and 710–764°C (~734°C) for the Yürükkaracaören sub-volcanic units. Apatite saturation temperatures range from 871 to 961°C (~906°C) for the Karakaya granite, from 846 to 960°C (~906°C) for the Topkaya granitoid and from 813 to 921°C (~861°C) for the Yürükkaracaören sub-volcanic units. The saturation temperatures were calculated for Karakaya and Topkaya enclaves, which can be considered as the mafic end members of the magma mixture, as 774–917°C and 735–905°C respectively. When the saturation temperatures are evaluated, it can be said that the magma mixture products started to crystallize from this temperature. According to the calculated results, it is seen that the zircon saturation temperatures are significantly lower. This is because this mineral is not seen in the early crystallization phase.

TRACE AND RARE EARTH ELEMENT VARIATIONS

An Ocean Ridge Granites (ORG) normalized spider diagram of magmatic rocks has been plotted. In this diagram, there is an enrichment of LIL elements (K, Rb, Ba), while there is a depletion in HFS (Th, Ta, Nb, Ce, Zr, Hf, Sm, Sm, Y, Yb) ele-

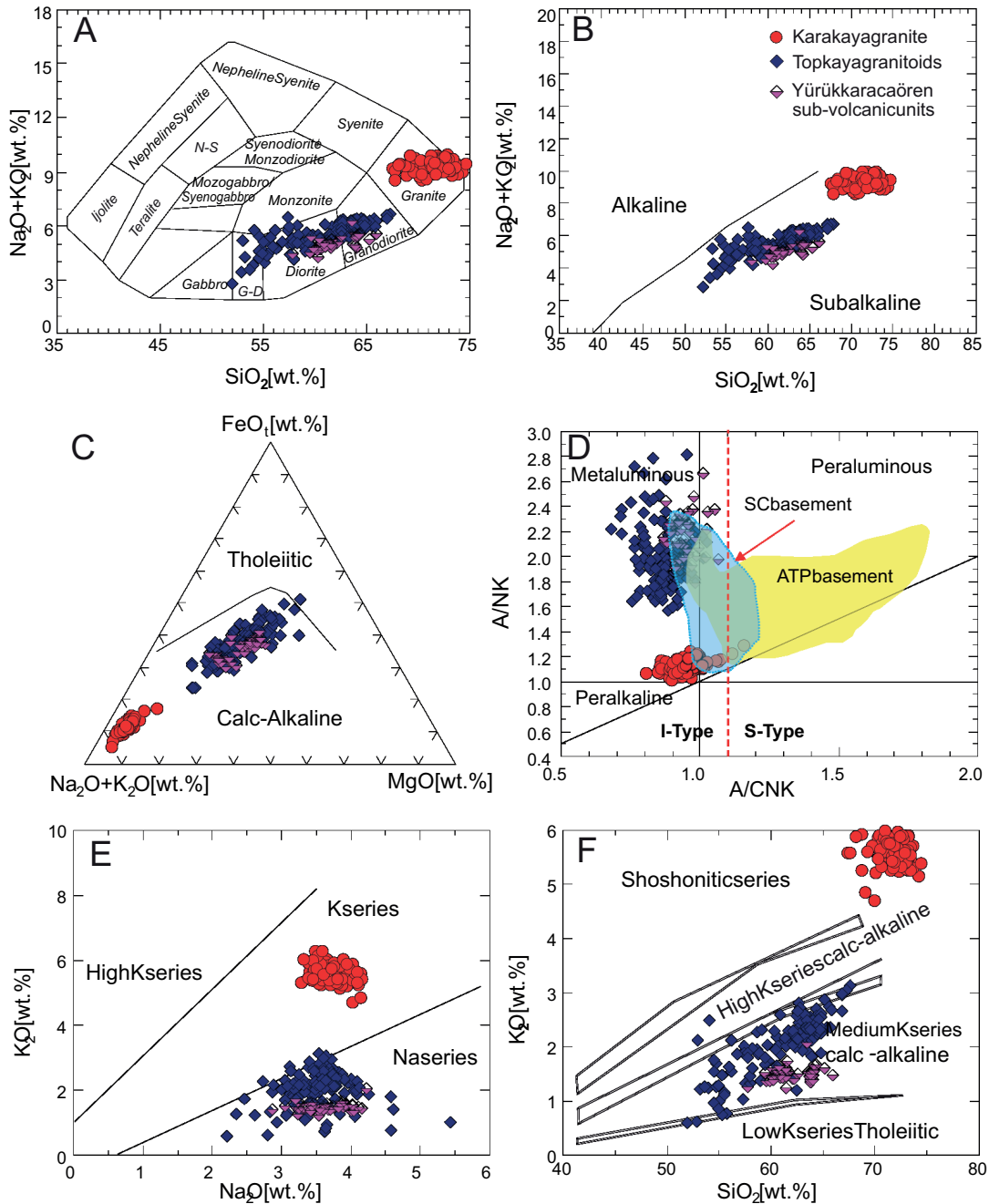


Fig. 4A – distribution of the magmatic rocks on a geochemical classification diagram (Cox et al., 1979); **B** – total alkali versus silica diagram and (C) AFM diagram (Irvine and Baragar, 1971); **D** – distribution of magmatic rocks on A/NK-A/CNK diagram (Shand, 1943; Maniar and Picolli, 1989); Sakarya Continent (SC) and Anatolite Tauride Platform (ATP) basement boundary is taken from Altunkaynak et al. (2012a); **E** – Na_2O versus K_2O diagram (Middlemost, 1975); **F** – K_2O versus SiO_2 diagram (Rickwood, 1989)

ments (Fig. 6A). The enrichments in Rb and Th in the granite is more than in the other magmatic units. This enrichment may be related to the fact that the Karakaya granite interacted more with the continental crust during emplacement and/or the presence of radioactive minerals such as zircon and allanite (orthite). On the other hand, there is a negative Ba anomaly indicating feldspar fractionation during the formation of the Karakaya granite.

All the magmatic units display enrichment in light rare earth elements (LREE) relative to heavy rare earth elements (HREE) in chondrite-normalized multi-element diagrams (Fig. 6B). In

the diagram, the enrichment in LREE in the granite is clearly higher than in the granodiorites and sub-volcanic units, which is considered to have been due to the greater degree of interaction of the Karakaya granite with the continental crust during its emplacement. While the distribution patterns of these multi-element diagrams prepared according to the trace elements and REE elements also support the original relation of the Topkaya granitoid and the Yürükcaracaören sub-volcanic rocks, they also indicated that Karakaya granite was derived from a magma source different from the Topkaya granitoid and the Yürükcaracaören sub-volcanic rocks.

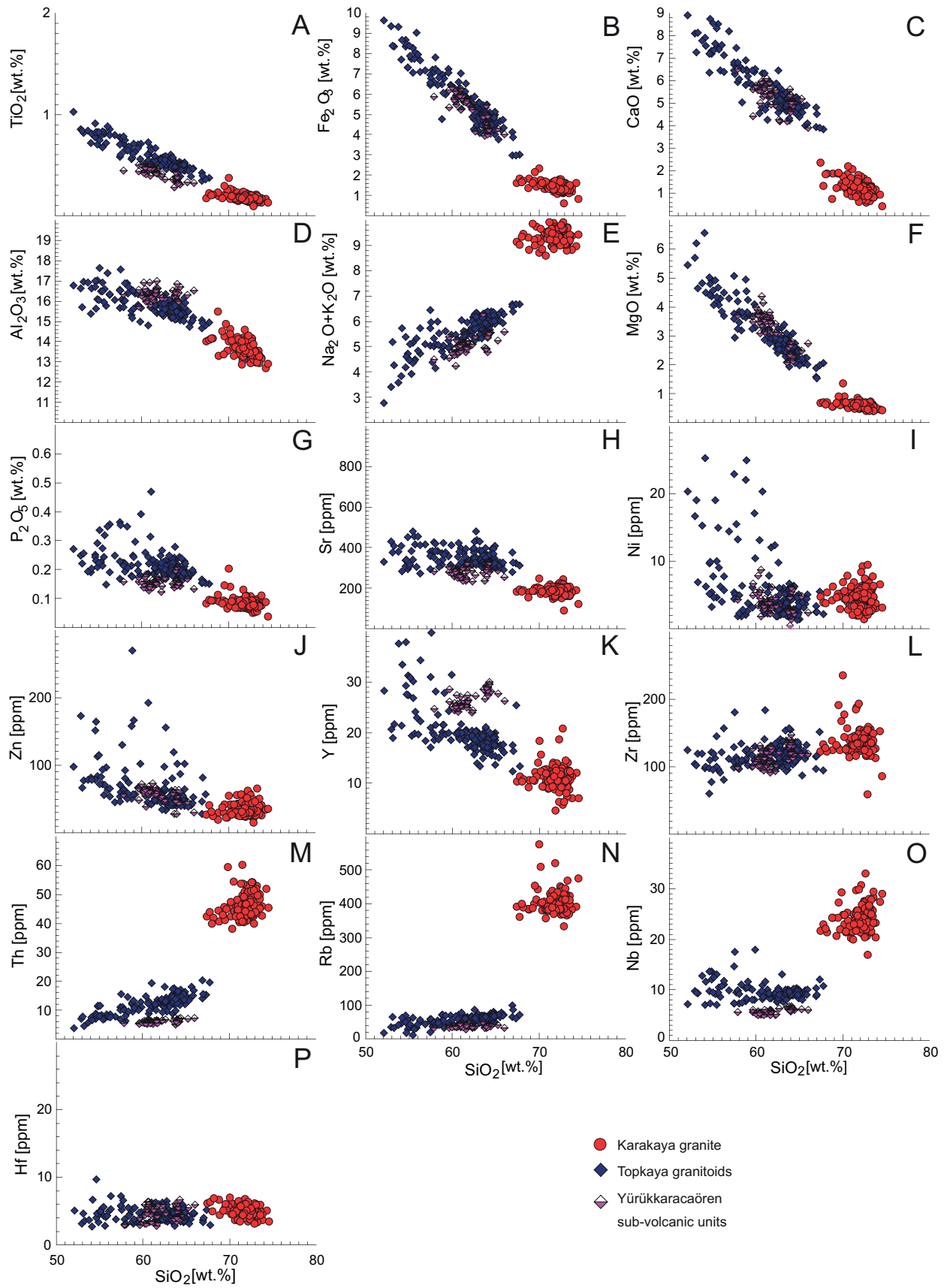


Fig. 5. Harker diagrams of selected major and trace elements

GEOCHRONOLOGY

The Ar-Ar method (performed on biotite and hornblende) was used for determining the crystallization ages of the magmatic units. The argon release values of the samples according to $^{40}\text{Ar}/^{39}\text{Ar}$ step-heating are given in [Appendix 2](#).

In the study; a 59.13 ± 1.87 Ma Ar-Ar weighted plateau and 59.55 ± 2.54 Ma inverse isochron age ([Fig. 7A, B](#)) were obtained from biotite for the granite (shoshonitic character), and a 44.30 ± 0.47 Ma Ar-Ar weighted plateau and 44.27 ± 0.48 Ma inverse isochron age ([Fig. 7C, D](#)) were obtained from the granodiorite and a 44.11 ± 0.89 weighted plateau and 43.88 ± 1.01 Ma inverse isochron age ([Fig. 7E, F](#)) were obtained from the sub-volcanic calc-alkaline rocks.

Nd AND Sr ISOTOPIC COMPOSITION

The Rb, Sr, Sm and Nd concentrations measured on all the magmatic units and $^{143}\text{Nd}/^{144}\text{Nd}$ and $^{87}\text{Sr}/^{86}\text{Sr}$ ratios are given in [Table 1](#). For the calculation of $(^{87}\text{Sr}/^{86}\text{Sr})_{\text{initial}}$, $(^{143}\text{Nd}/^{144}\text{Nd})_{\text{initial}}$, ϵSr , ϵNd , $(\epsilon\text{Sr})_{\text{initial}}$ and $(\epsilon\text{Nd})_{\text{initial}}$ values, the emplacement ages of 44.11 Ma for the Topkaya and Yürükkaracaören magmatic rocks and 59.13 Ma for the Karakaya granite were used ([Table 1](#)).

DISCUSSION

NATURE OF THE MAGMAS

Geochemical and isotope data were used to determine the origin of the intrusive rocks. In the discrimination diagram of the magma forming the intrusive units, it is seen that all the samples reflect an orogenic nature ([Wilson and Bianchini, 1999](#); [Krmíček et al., 2011](#); [Fig. 8](#)).

Considering the Rb fractionation index, significant differences in Rb (419 to 575 ppm for Karakaya; 37 to 80 ppm for Topkaya-Yürükkaracaören) point to differences in the magma sources that formed the Karakaya and Topkaya-Yürükka-

caören rock groups. The geochronological data and geochemical discrimination diagrams also support these suggestions.

The Sr and Nb isotope ratios of the Karakaya and Topkaya-Yürükkaracaören units reveal that their respective magmas cannot be derived from the same source magma. The Karakaya granite differs from the Topkaya and Yürükkaracaören magmatic units in its higher $(^{87}\text{Sr}/^{86}\text{Sr})_i$ (0.7096436–0.7109025) and lower $(^{143}\text{Nd}/^{144}\text{Nd})_i$ (0.512178–0.512243) isotopic ratios. Although the low $(^{87}\text{Sr}/^{86}\text{Sr})_i$ (0.7055928–0.7061354) and high $(^{143}\text{Nd}/^{144}\text{Nd})_i$ (0.512502–0.512594) values of the Topkaya and Yürükkaracaören units indicate an Ocean Island Basalt (OIB)-like magma source ([Fig. 9](#)), the same isotopic signature may be indicative of typical Volcanic Arc magmas. The low ϵNd and relatively higher Mg# values of the Topkaya and Yürükkaracaören magmatic units indicate a magma derived from a continental lithospheric mantle source. Furthermore, low ϵNd and $^{87}\text{Sr}/^{86}\text{Sr}$ ratios of the Topkaya and Yürükkaracaören magmatic rocks indicate that metasomatized mantle can be a source. These isotopic ratios may represent different magma sources and/or different degrees of continental contamination. On the Zr/Nb-Zr diagram, it is seen that the magmas forming all magmatic units were widely exposed to crustal contamination during crystallization ([Fig. 10A](#)). Sr isotope ratios are seen in the $^{87}\text{Sr}/^{86}\text{Sr}$ versus Sr diagram ([Briqueu and Lancelot, 1979](#); [Nelson, 2003](#)); while crustal contamination of ~40–60% is inferred during the emplacement of the magma forming the Topkaya and Yürükkaracaören magmatic units, this ratio rises to >80% in the Karakaya granite ([Fig. 10B](#)).

Magmatic rocks of study area have been plotted on Th/Yb versus Ta/Yb diagrams ([Pearce et al., 2005](#)) with the aim of revealing the magma source ([Fig. 11A](#)). These ratios are almost independent of the effects of fractional crystallization and partial melting. Th/Yb and Ta/Yb ratios may indicate magma source variations and crustal assimilation. The high Th/Yb ratios in the magmatic units of the study area, which have similar distributions to the Eocene granitic rocks of north-west Anatolia, are remarkable. An increase in Th/Yb ratios caused by enrichment in Th content (average 46.6 ppm in the Karakaya granite, 12.4 ppm in the Topkaya granitoid and 6.2 ppm in the Yürükkaracaören sub-volcanic rocks) may be explained by subduction-related processes and metasomatism of mantle material. Subduction components cause enrichment of Th rather than of Ta and Yb. In addition, crustal contamination can increase the Th/Yb ratio.

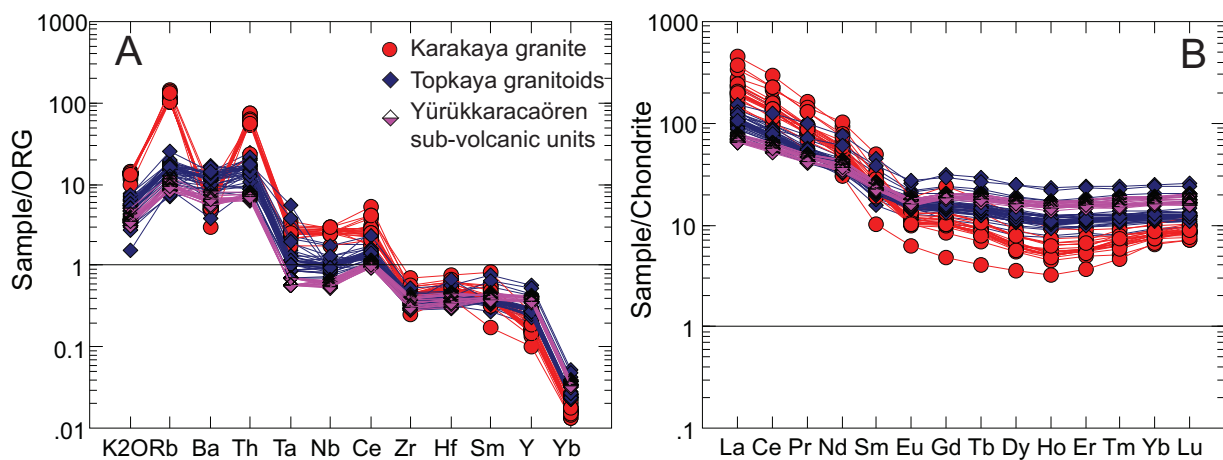


Fig. 6A – multi-element diagrams of the magmatic rocks on ORG-normalized trace element;
B – chondrite-normalized REE diagrams (ORG values from [Pearce et al., 1984](#);
 chondrite values from [Evensen et al., 1978](#))

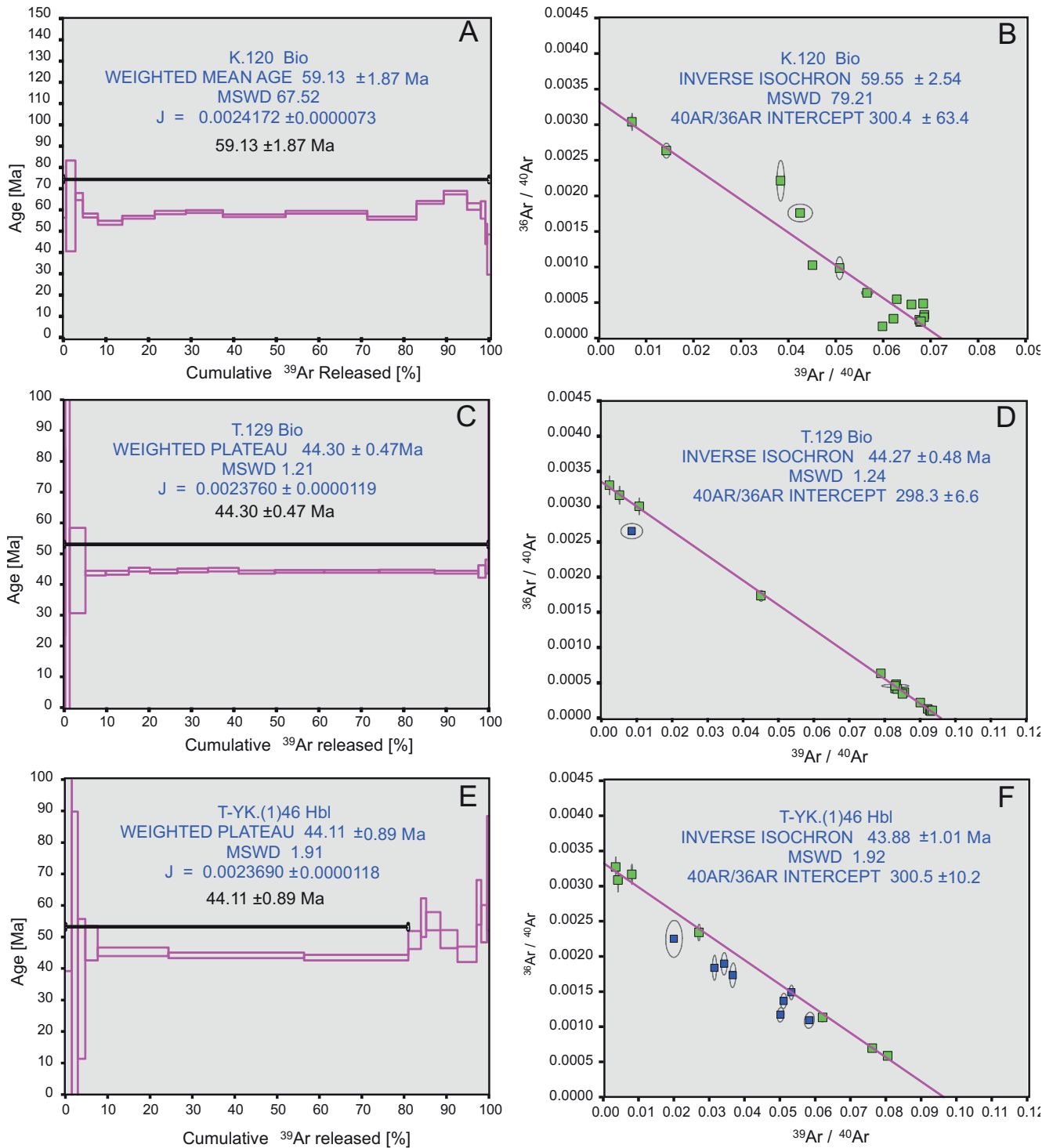


Fig. 7A – Ar/Ar weighted plateau; B – inverse isochron age graphics of the Karakaya granite; C – Ar/Ar weighted plateau; D – inverse isochron age graphics of the Topkaya granitoid; E – Ar/Ar weighted plateau; F – inverse isochron age graphics of the Yürükkaracaören sub-volcanic rocks

The distinction between source contamination and crustal assimilation can be more easily defined by using the Th/Y versus Nb/Y diagram (Pearce, 1983). On the Th/Y versus Nb/Y diagram, all granitoid samples plot along a line with Th/Nb = 1, reflecting a magma source which was affected by subduction zone enrichments (Fig. 11B). Similarly, it is seen that the parental magma source forming the Topkaya granodiorite and

Yürükkaracaören sub-volcanic rock groups may be enriched in subduction-related and/or crustal compounds according to the Rb/Y versus Nb/Y diagram (Edwards et al., 1991). In addition, it is clear that within-plate enrichment is also efficient, as well as subduction/crust interaction, on the magma source forming the Karakaya granites (Fig. 12A).

Table 1

Isotopic ratios of the magmatic rocks in the study area

Samples	Loc.	Unit	Age [Ma]	M E A S U R E D							C A L C U L A T E D				
				$^{87}\text{Sr}/^{86}\text{Sr}$	$^{143}\text{Nd}/^{144}\text{Nd}$	Rb	Sr	Sm	Nd	$(^{87}\text{Sr}/^{86}\text{Sr})$	$(^{143}\text{Nd}/^{144}\text{Nd})$	ϵSr	ϵNd	$(\epsilon\text{Sr})_{\text{initial}}$	$(\epsilon\text{Nd})_{\text{initial}}$
K-192	KK	*	59.13	0.716645 ±3	0.512233 ±5	575.7	246.0	7.60	49.1	0.710902	0.512178	168.061862	-7.900312	87.630284	-7.489175
K-168	KK	*	59.13	0.714492 ±5	0.512291 ±5	419.3	222.8	3.93	28.9	0.709886	0.512243	137.514188	-6.768909	73.210158	-6.227505
K-76	KK	*	59.13	0.715306 ±5	0.512278 ±5	424.6	183.7	3.93	35.1	0.709644	0.512238	149.063564	-7.022499	69.767606	-6.314886
AK-49	TK	**	44.30	0.705915 ±4	0.512632 ±15	65.8	370.5	3.52	24.8	0.705593	0.512594	15.820091	-0.117042	12.026864	0.258376
T-68	TK	**	44.30	0.706310 ±5	0.512602 ±5	39.6	411.7	3.94	19.5	0.706135	0.512548	21.424518	-0.702250	19.725990	-0.638599
T-86	TK	**	44.30	0.706244 ±5	0.512606 ±12	67.8	314.3	3.42	19.8	0.705853	0.512560	20.488082	-0.624222	15.711768	-0.408515
T-108	TK	***	44.11	0.706056 ±4	0.512618 ±12	75.8	360.9	3.00	17.6	0.705677	0.512573	17.820658	-0.390139	13.211701	-0.163600
T-11	TK	****	44.11	0.706074 ±5	0.512617 ±6	80.5	395.3	3.45	18.8	0.705706	0.512568	18.076050	-0.409646	13.630734	-0.250516
YK-6	YKÖ	*****	44.11	0.705742 ±7	0.512581 ±3	42.6	325.6	4.09	20.3	0.705506	0.512528	13.365494	-1.111896	10.787548	-1.045597
YK-42	YKÖ	*****	44.11	0.706194 ±7	0.512557 ±9	39.0	326.7	3.68	17.6	0.705978	0.512502	19.778661	-1.580062	17.493132	-1.553115
YK-78	YKÖ	*****	44.11	0.706131 ±5	0.512589 ±19	37.8	285.3	3.48	17.4	0.705892	0.512536	18.884790	-0.955840	16.263177	-0.881897

Standard errors belong to the last one or two steps, SRM987 standard was measured as 0.710260 ± 5 ($n = 2$) during the measurement period and Sr isotope measurement results were corrected according to this value (* – granite, ** – diorite porphyry, *** – microcrystalline diorite porphyry, **** – fine-grained diorite porphyry, ***** – microcrystalline granodiorite porphyry) Sr abundance, Sr isotope mass and Sr-Rb atomic weight from Faure (1986); Nd isotope ratios from Wasserburg et al. (1981); Sm isotope ratios from Russ et al. (1971), Jacobsen and Wasserburg (1980); Nd isotope mass and Sr-Nd isotope ratios from Wapstra and Bos (1977)

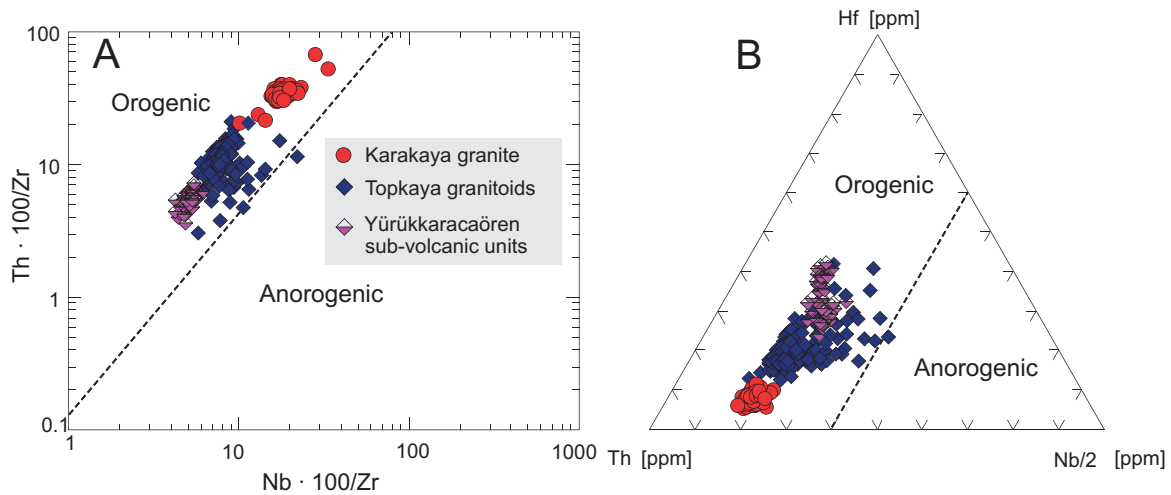


Fig. 8A – distribution of magmatic rocks on $\text{Th} \cdot 100/\text{Zr}$ versus $\text{Nb} \cdot 100/\text{Zr}$ (Wilson and Bianchini, 1999);
B – Th-Hf-Nb/2 diagrams (Krmíček et al., 2011)

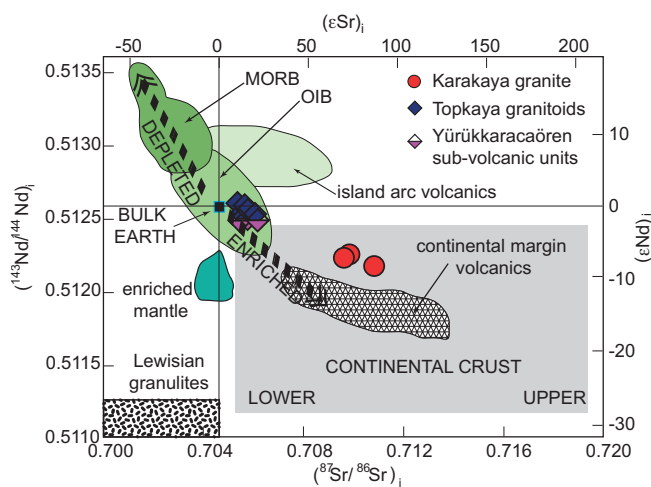


Fig. 9. Sr-Nd isotopic correlation diagram of the magmatic rocks in the study area (field lines are taken from Zindler and Hard, 1986; Faure, 1986)

CRYSTALLIZATION EVOLUTION OF MAGMAS AND MIXING

A Sr versus MgO diagram, which shows the controls on the crystallization of ferromagnesian minerals at medium to high temperatures, can be used to evaluate the crystallization of magmas. The Sr versus MgO distribution diagram here shows that the crystallization of magma forming the granodiorite and sub-volcanic magmatic units was controlled by ferromagnesian minerals. Feldspar played an important role during the crystallization of the granite magma (Fig. 12B).

Moreover, Fe_2O_3 , CaO, Al_2O_3 , MgO depletions in the residual magma could be explained by the crystallization of Ca-rich plagioclases and mafic minerals such as amphibole, biotite and partly pyroxene. P_2O_5 and TiO_2 are consumed by the retention in accessory minerals such as apatite and ilmenite (Mason and Moore, 1966).

SiO_2 versus $\text{CaO}/(\text{CaO} + \text{Na}_2\text{O})$ and SiO_2 versus $\text{MgO}/(\text{MgO} + \text{Fe}_2\text{O}_3)$ diagrams have been used to reveal the source and fractionation of a magma (Fig. 13A, B). The Topkaya granitoid and Yürükkaracaören sub-volcanic rocks are the crystallization products of magmas originally related to each other. But, it is clearly seen that in the diagrams the Karakaya granite is derived from a magma source different from that of the Topkaya granitoid and Yürükkaracaören sub-volcanic rocks. During fractionation, $\text{CaO}/(\text{CaO} + \text{Na}_2\text{O})$ and $\text{MgO}/(\text{MgO} + \text{Fe}_2\text{O}_3)$ concentrations should produce exponential trends with increasing SiO_2 (Johnston, 2001). However, the $\text{CaO}/(\text{CaO} + \text{Na}_2\text{O})$ and $\text{MgO}/(\text{MgO} + \text{Fe}_2\text{O}_3)$ concentrations show linear trends with increasing SiO_2 . These linear relationships provide evidence of mixing.

The presence of some specific textures within the host rock and enclaves points to coeval crystallization and magma mixing (Slaby and Martin, 2008). Also the presence of microgranular enclaves of various sizes with different compositions in the host rocks may reflect the nature of the Karakaya and Topkaya granitoid, showing various chemical compositions within the discrimination diagrams. The development of some specific textures in the magmatic rocks of the study area is also a fingerprint of magma mixing, which may also be revealed by geochemical discrimination diagrams.

When felsic magma and more mafic magmas are mixed, some specific textures may result, such as the poikilitic K-feldspar, quartz-hornblende ocellar texture and small lath-shaped plagioclases inside coarse plagioclases (see Petrology section) (Didier and Barbarin, 1991) observed in the magmatic rocks of the study area. When felsic and relatively more mafic magmas are mixed in melt form, fine-grained calcic plagioclase, hornblende and/or biotite minerals occur in the hybrid system. K-feldspars containing these fine crystals or coarse plagioclases containing small lath-shaped plagioclases as inclusions can form in an equilibrated hybrid system. Additionally, quartz may crystallize in the early phase of mixing and form a cooling surface for some mafic minerals in the equilibrated hybrid system. Thus, fine-grained mafic minerals attached around quartz crystals can be observed (Hibbard, 1991).

Crystalline differentiation and/or continental contamination may also affect crystallization after the mixing of magmas. When a Y versus Rb diagram, expressing crystal differentiation tendencies, is considered according to the mineral crystalliza-

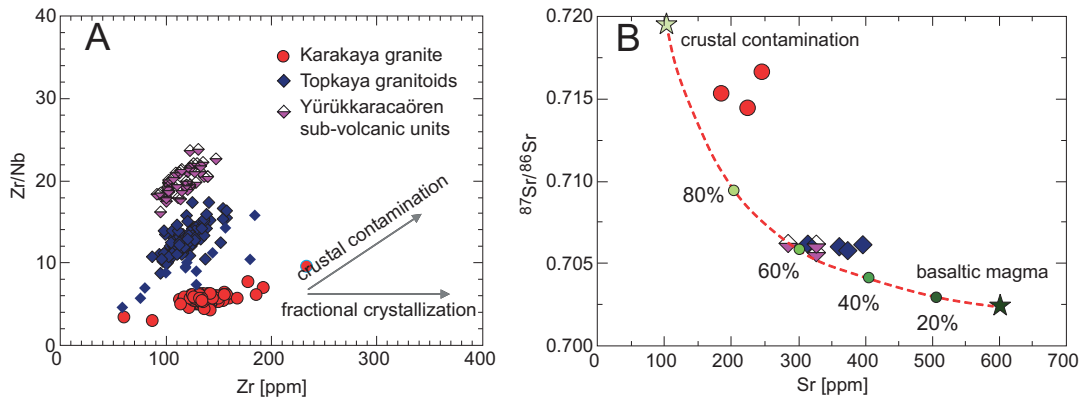


Fig. 10A – distribution of the magmatic rocks on Zr/Nb-Zr diagram; **B** – $^{87}\text{Sr}/^{86}\text{Sr}$ -Sr diagrams defining approximate crustal contamination rates

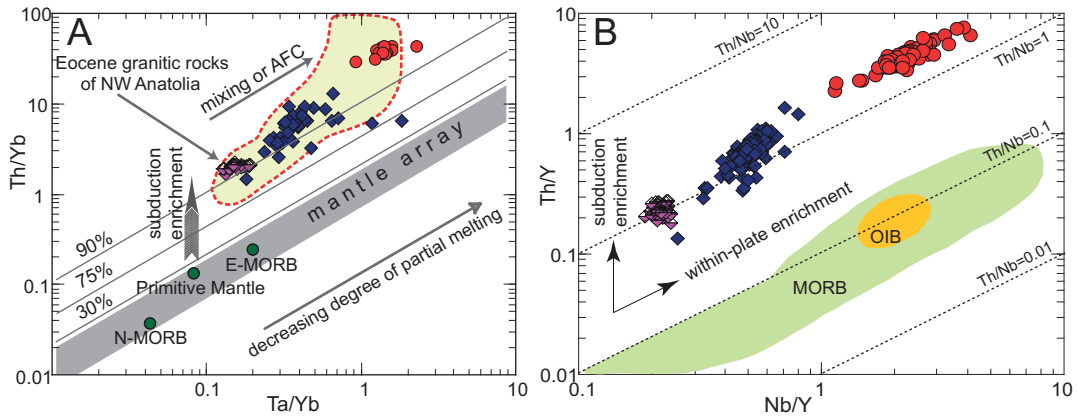


Fig. 11A – distribution of the magmatic rocks on a Th/Yb versus Ta/Yb diagram (Pearce et al., 2005) (NW Anatolia Eocene granitic rock boundaries are taken from Altunkaynak et al., 2012b); **B** – distribution of the magmatic rocks on a Th/Y versus Nb/Y diagram (Pearce, 1983)

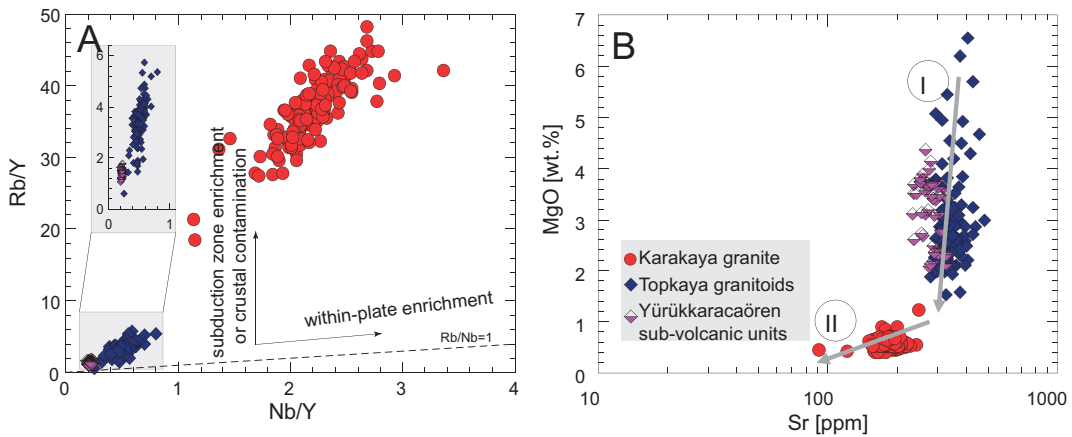


Fig. 12A – Rb/Y versus Nb/Y diagram (Edwards et al., 1991); **B** – distribution of the magmatic units on a MgO versus Sr crystal differentiation diagram (I – differentiation trend of ferromagnesian minerals, II – differentiation trend of feldspar minerals)

tion of the magmatic units as revealed by Keskin (2002), it is seen that the granite samples are in close relation with the differentiation vector 7. In this situation; it may be said that the magma giving rise to granite of felsic composition shows conformity to a 30% amphibole, 40% plagioclase, 20% biotite and 10% quartz crystal differentiation tendency. It has been observed in the same diagram that the other rock groups show tendencies in parallel with the vector 5. Forty percent amphibole, 50% plagioclase, 5% clinopyroxene and 5% orthopyroxene crystal differentiation is foreseen for this magma of intermediate character (Fig. 13C).

Pearce et al (1984) proposed Rb-(Yb + Ta) and Rb-(Y + Nb) diagrams to determine the tectonic setting of granitoids. On the Rb-(Yb + Ta) and Rb-(Y + Nb) diagrams, the Karakaya granite show syn-COLG characteristics, whereas granodiorite and sub-volcanic units exhibit VAG characteristics (Fig. 14A, B). On the other hand, in the Hf-Rb/30-Ta · 3 triangular diagram suggested by Harris et al. (1986), the granites are of collision character, while the other magmatic units show collision-related arc granitoid character (Fig. 14C). Although the Karakaya granite plots on the syn-collision part of the tectonic discrimination diagrams, the presence of possibly more mafic end-member MMAs within the granites may imply a lower continental crust-like source. MMAs in the Karakaya granite indicate the presence of a more mafic end member. Because the Karakaya granite samples plot along a line with Th/Nb = 1 (see Nature of the Magmas section), the mafic magma injections into the continental crust may actually be explained as volcanic arc and enriched within-plate occurrences. These more mafic magmas may rise through

TECTONIC REGIME

Immobile trace elements such as Ti, Zr, Y, Nb and Hf can be used to classify magmatic rocks according to their tectonic setting (Pearce and Cann, 1973; Pearce et al., 1984; Pearce,

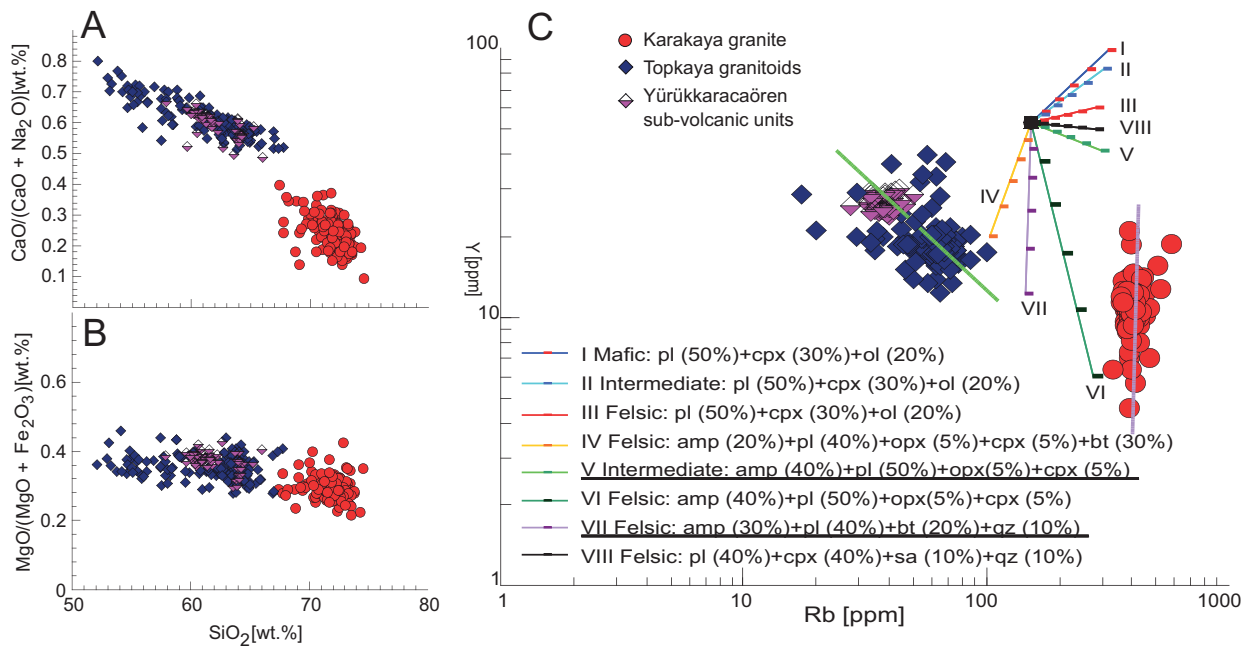


Fig. 13A – distribution of the magmatic rocks on CaO/(CaO + Na₂O) versus SiO₂; (B) MgO/(MgO+Fe₂O₃) versus SiO₂ and (C) Y versus Rb diagrams for modelled general direction of crystal differentiation (Keskin, 2002)

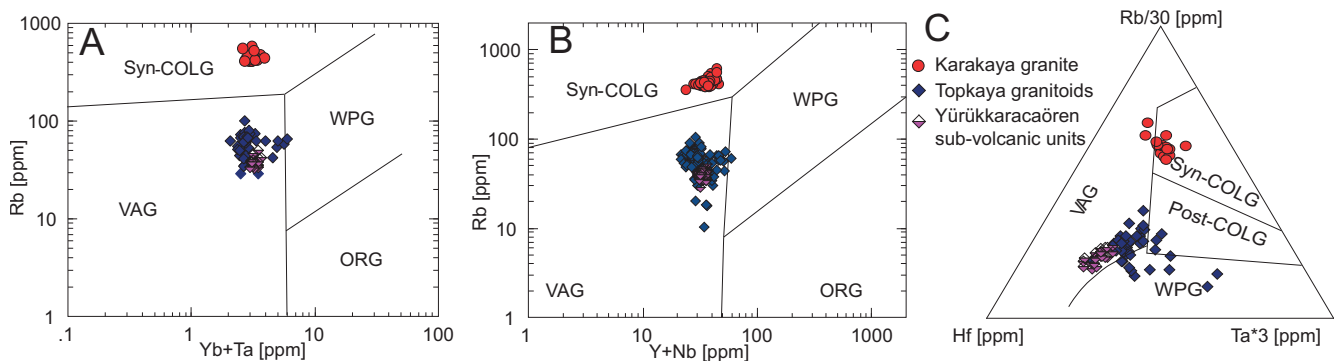


Fig. 14A – distribution of the magmatic rocks on Rb-Yb + Ta; B – Rb-Y + Nb and C – Hf-Rb/30-Ta · 3 tectono-magmatic discrimination diagrams

the continental crust, heating and partially melting it (Shellnutt et al., 2011; Zheng et al., 2016 and references therein). The melting of continental crust may in consequence produce Syn-Colg character granitic rocks in the region.

GEODYNAMIC EVOLUTION OF THE MAGMATIC UNITS

Comparison of the rock units representing the magmatism developing during closure of the northern branch of the Neo-Tethys after the collision of the Anatolide-Tauride Platform with the Sakarya Continent (Harris et al., 1994; Altunkaynak, 2007; Altunkaynak et al., 2012a; Karslı et al., 2020) is given in Table 2. All magmatic units (Karakaya granite, Topkaya granitoid and Yürükkaracaören sub-volcanites) are located among the northwestern Anatolian Suture Zone granitoids (Altunkaynak, 2007) or northwestern Anatolia southern belt granitoids (Altunkaynak et al., 2012a) and it is accepted that they were formed as a result of similar geological events. These magmatic suites show changes from calc-alkali to high K calc-alkali (Köprubaşı and Aldanmaz, 2004; Okay and Satır, 2006; Karacık et al., 2008; Sunal et al., 2019) and even to shoshonitic composition (Altunkaynak et al., 2012b). The granodiorite and sub-volcanic units are Na series-calc-alkaline in character, while the granite shows a shoshonitic character. Although the Karakaya granite does not show alkaline tendency in the main element oxide discrimination diagrams, its alkaline enclave and fluorite content are interpreted as traces of alkali magma contribution.

Petrographic, geochemical, isotopic and radiometric data from the study area show that the Yürükkaracaören sub-volcanic units show very similar properties to the Topkaya granodiorites; in close relation with Topkaya pluton, they could be sub-volcanic apophyses of the Topkaya pluton. Similarly, there are many volcanic equivalents of Eocene plutons in northwestern Anatolia to the north of the İzmir-Ankara-Erzincan Suture Zone (Keskin et al., 2008; Altunkaynak and Dilek,

2013; Ersoy and Palmer, 2013; Gülmez et al., 2013; Elmas et al., 2016; Kasapoğlu et al., 2016; Sunal et al., 2019; Göçme-nçil et al., 2019).

The geological-petrological-geochemical and geochronological data lead to a geodynamic evolution model suggested for the formation of the magmatic rocks of the study area.

The closure of the northern and southern branches of Neo-Tethys have been very influential in shaping the geological structure of Turkey. This closure and continent-continent collision are known to have continued until the end of the Late Cretaceous and even until the Paleocene (~70 Ma; Fig. 15A). The subduction of the Neo-Tethys from the Middle Triassic to the Cretaceous (Okay, 2011) towards the north and the isotopic ages taken from blueschist and eclogites indicate an Albian (~105 Ma) age (Okay et al., 2006).

Altunkaynak (2007) suggested that the age of suture zone granitoids in northwestern Anatolia is between 52–48 Ma. This study shows that Karakaya granite is 59.13 ± 1.87 Ma old. Therefore, it is thought that the suture zone granitoids may be between 60–48 Ma old. Mafic magma may have been present at the lower continental crust-upper mantle boundary (dominantly lower continental crust-like character) together with intense heat transfer from an asthenospheric window opened as a result of the sinking lithospheric slab during this interval (Fig. 15B; Okay and Satır, 2006; Altunkaynak et al., 2012a). The Anatolide-Tauride Platform collision with the Sakarya Plate related to the closure of the Neo-Tethys and continental crust thickness has increased in the collision zone. The magma upwelling as a result of the resulting partial melting in the lower crust strongly interacted with the continental crust (~80% in the model diagram plotted according to the isotopic data). This may have produced magma of very acidic character. It is possible also that this acid magma formed the granites at this stage.

Post-collisional VAG character magmatic rocks are observed in different parts of north-west Anatolia, on the boundary of the Tavşanlı-Sakarya Zone and within the Tavşanlı Zone during the Eocene (48–34 Ma; Altunkaynak, 2007; Okay, 2011). At

Table 2

Comparative petrological-petrogenetic characteristics of the magmatic units

	Granite (Karakaya)	Granodiorite (Topkaya)	Sub-volcanic unit (Yürükkaracaören)
Rock type	tourmaline/biotite granite	granodiorite/diorite porphyry	diorite porphyry/ microdiorite porphyry
Enclave	alkaline character microgranular	mafic microgranular	mafic microgranular (rare)
Dyke	aplites	aplites+mafic dykes	mafic dykes
Contact relationship	closely contact with ophiolites	closely contact with ophiolites	closely contact with ophiolites
	tectonic contact with metamorphic rocks	closely contact with metamorphic rocks	not observed
Magma character	metaluminous/ shoshonitic and K series	metaluminous/calc-alkaline and Na series	metaluminous/ calc-alka- line and Na series
Tectonic discrimination	collision-related granitoids (Syn-Colg)	collision-related arc granitoids (Post-Colg)	collision-related arc granitoids (Post-Colg)
Assimilation/contamination	crustal interaction is too high	crustal interaction is low	crustal interaction is low
ϵ_{Nd}	-6.7/-7.9	-0.1/-0.7	-0.9/-1.1
$^{87}Sr/^{86}Sr$	0.714-0.716	0.705-0.706	0.705-0.706
Ar/Ar age	59.13 Ma (Selandian)	44.3 Ma (Lutetian)	44.11 Ma (Lutetian)
Magma source	derived from a magma generated at the lower continental crust-upper mantle boundary; collision-subduction related	subduction-related partial melting of lithospheric mantle-like source	differantiation from the main granitoid magma
Emplacement	deep	deep and shallow	shallow

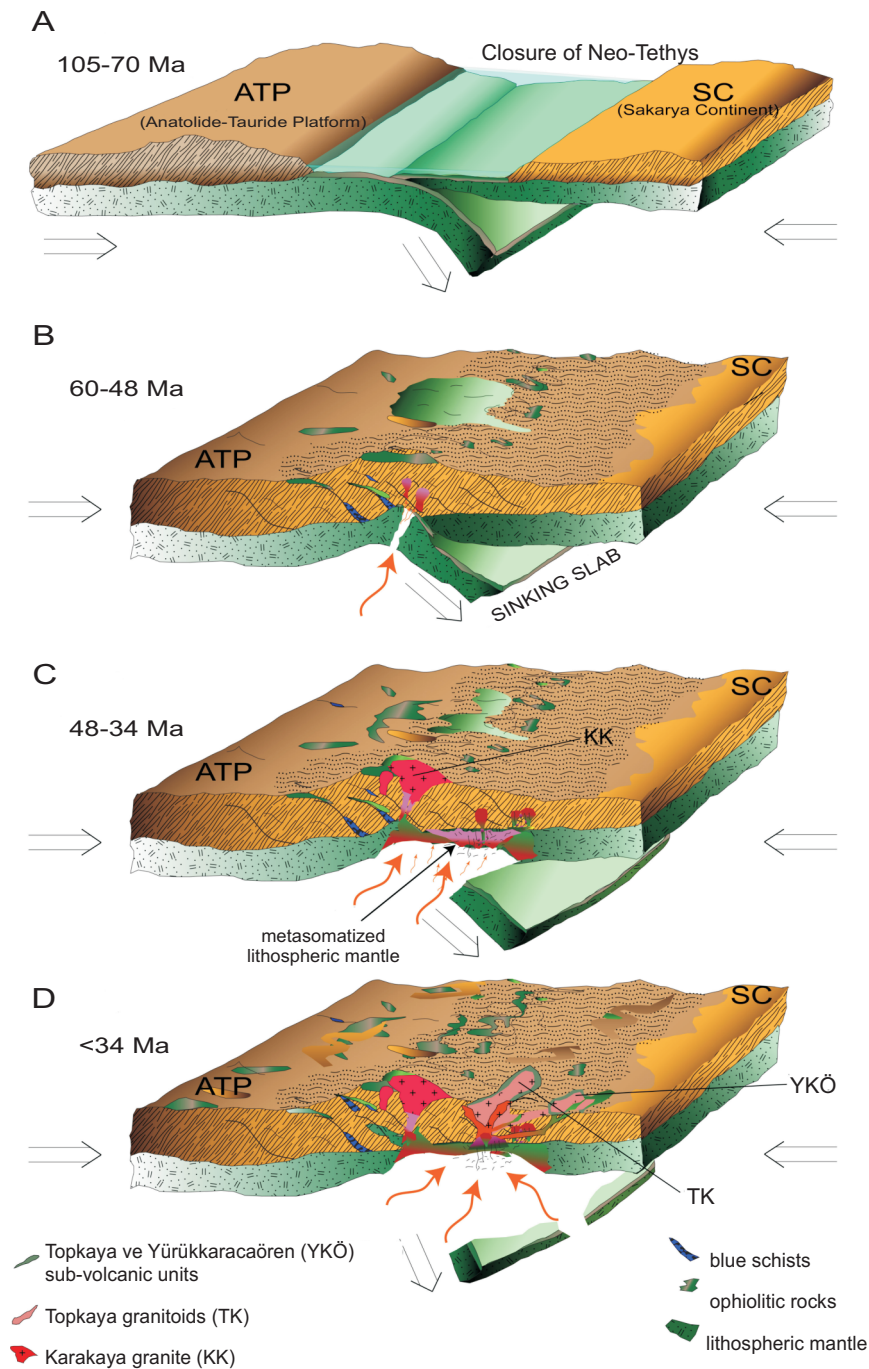


Fig. 15. Schematic model of geodynamic evolution of the magmatic units in the study area

this time, mafic magma has formed which partial melting of the continental lithospheric mantle associated with asthenospheric upwelling during delamination of the sinking lithospheric slab after the collision (Fig. 15C). Various interactions developed between this mafic magma, derived from the upper mantle, and the more felsic magma derived from the lower continental crust (Fig. 16A), in the form of thermal, chemical and mechanical changes, depending on the rheological properties of these magmas at different depths in the crust. In this phase, responsible for the formation of granodiorite and sub-volcanic units, magma emplacement in the continental crust turned towards a

more felsic character with continental crust interaction (~40–50% in the model diagram plotted according to the isotope data). However, the partial melting that continued in the lower continental crust continually fed this magma chamber (Fig. 16B). At this stage, magma mixing occurred together with chemical changes in the mafic and felsic magmas. Thus, a hybrid calc-alkaline granodioritic magma formed leading to various microscopic textural features associated with the thermal changes taking place at this stage. At the same stage, mafic granular textured enclaves developed as a result of the magma mingling, with intense mechanic interaction of the mafic and fel-

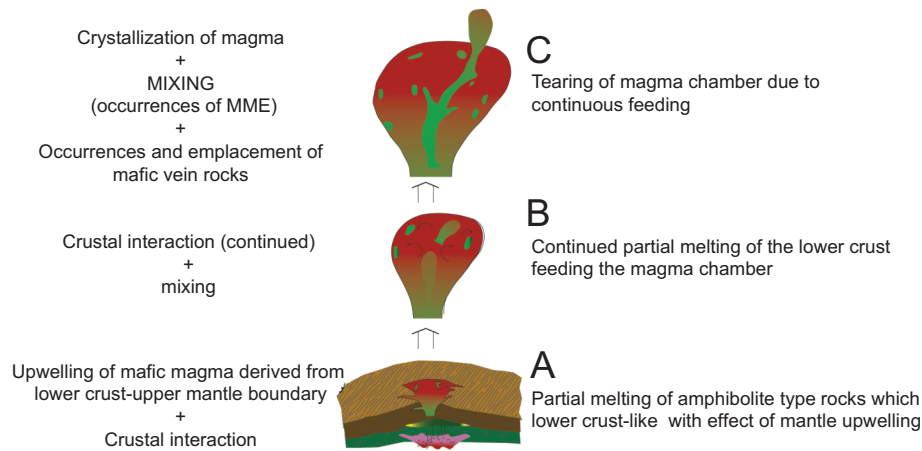


Fig. 16. An emplacement model for the granodiorite and sub-volcanic magmatic units

sic magmas. The magma chamber, continuously fed, grew towards the end of the third phase and during this, rupture of the magma chamber was able to occur (Fig. 16C). Magma flow occurred towards the outside from the ruptured magma chamber, cutting through both the granodiorite bedrock and diorite porphyry sub-volcanic rocks. It is inferred that the mafic to intermediate vein rocks characterized by microgabbro porphyry/acidular amphibole diorite porphyry compositions may have begun to form during this phase.

Surface processes of these rocks, with erosion and uplift, may have begun when emplacement of the intrusive units in the study area was completed (Fig. 15D).

CONCLUSION

The collision of the Tavşanlı and Sakarya zones, during subduction after consumption of the Neo-Tethys, started in the Paleocene. This continental collision produced a heterogeneous mantle that would generate magmas related to the collision in central-northwestern Anatolia. This heterogeneous mantle source may have formed a resource for the magmatism that began in the Paleocene in different parts of the region. A $^{40}\text{Ar}/^{39}\text{Ar}$ radiometric age from biotite of the Karakaya granite yielded a cooling age of 59.13 ± 1.87 Ma, while amphiboles from the Topkaya granodiorite and Yürükaracaören sub-volcanic rocks gave cooling ages of 44.3 ± 0.47 and 44.11 ± 0.89 Ma respectively. The Karakaya magmatic units are rep-

resented by collision-related magmatic rocks and the Topkaya and Yürükaracaören magmatic units represent arc-related magma products. The geochemical element distribution and isotopic data of the granodiorites are quite similar to those of the sub-volcanic samples. This may indicate a similar magma origin injected as different stocks in the region. The petrographical textures of the Yürükaracaören subvolcanic rocks may represent the upper part of the Topkaya granitoid in the study area. It is clear that the granite forms the first magmatic product along the northwestern section of the İzmir-Ankara-Erzincan Suture Zone. This suggests that the closure evolution of the Neo-Tethys in the northwestern Anatolia follows a scissor-shaped pattern from the east towards the far west of the closure.

All geological, petrographical, geochemical, isotopic and geochronological data indicate that the granites formed before the granodiorites and subvolcanic units. Subduction-related magma caused the formation of the Karakaya, Topkaya and Yürükaracaören granitic bodies in the same geodynamic regime though with different textural features and mineral composition.

Acknowledgements. This study was supported by the Ministry of Development under grant number 2012K120440 and Ankara University Research Project BAP-09B-4343-016. We would like to thank Ankara University, Directory of Earth Science Applications and Research Center-YEBIM and all its employees for their support of this study. We also thank the reviewers for their efforts to improve the article.

REFERENCES

- Aldanmaz, E., Pearce, J., Thriwall, M.F., Mitchell, J., 2000.** Petrogenetic evolution of late Cenozoic, postcollision volcanism in western Anatolia, Turkey. *Journal of Volcanology and Geothermal Research*, **102**: 67–95.
- Altınlı, İ.E., 1973.** Orta Sakarya'nın Jeolojisi (in Turkish). 50th Anniversary of the Republic, Earth Sciences Congress, Ankara: 159–190.
- Altunkaynak, Ş., 2007.** Collision-driven slab breakoff magmatism in northwestern Anatolia, Turkey. *The Journal of Geology*, **115**: 63–82.
- Altunkaynak, Ş., Dilek, Y., 2006.** Timing and nature of post collisional volcanism in Western Anatolia and geodynamic implications. *GSA Special Paper*, **409**: 321–351.
- Altunkaynak, Ş., Dilek, Y., 2013.** Eocene mafic volcanism in northern Anatolia: its causes and mantle sources in the absence of active subduction. *International Geology Review*, **55**: 1641–1659.
- Altunkaynak, Ş., Dilek, Y., Genç, C.Ş., Sunal, G., Gertisser, R., Furnes, H., Foland, K.A., Yang, Y., 2012a.** Spatial, temporal and geochemical evolution of Oligo–Miocene granitoid magma-

- tism in western Anatolia, Turkey. *Gondwana Research*, **21**: 961–986.
- Altunkaynak, Ş., Sunal, G., Aldanmaz, E., Genç, C.Ş., Dilek, Y., Furnes, H., Foland, K.A., Yang, J., Yıldız, M., 2012b.** Eocene granitic magmatism in NW Anatolia (Turkey) revisited: new implications from comparative zircon SHRIMP U-Pb and ^{40}Ar - ^{39}Ar geochronology and isotope geochemistry on magma genesis and emplacement. *Lithos*, **155**: 289–309.
- Aydoğan, M.S., Coban, H., Bozcu, M., Akıncı, Ö., 2008.** Geochemical and mantle-like isotopic (Nd, Sr) composition of the Baklan Granite from the Muratdağı Region (Banaz, Uşak), Western Turkey: implications for input of juvenile magmas in the source domains of western Anatolia Eocene–Miocene granites. *Journal of Asian Earth Sciences*, **33**: 155–176.
- Aysal, N., Şahin, S.Y., Güngör, Y., Peytcheva, I., Öngen, S., 2018.** Middle Permian–early Triassic magmatism in the Western Pontides, NW Turkey: geodynamic significance for the evolution of the Paleo-Tethys. *Journal of Asian Earth Sciences*, **164**: 83–103.
- Bağcı, M., Demirbilek, M., İlbeyli, N., Yıldız, A., Kibici, Y., 2019.** Geochronological and geochemical constraints and origin of the Tavşanlı Zone plutonic rocks (NW Turkey). *Turkish Journal of Earth Sciences*, **28**: 60–84.
- Ballouard, C., Poujol, M., Boulvais, P., Branquet, Y., Tartèse, R., Vigneresse, J.L., 2016.** Nb-Ta fractionation in peraluminous granites: a marker of the magmatic-hydrothermal transition. *Geology*, **44**: 231–234.
- Briquet, L., Lancelot, J.R., 1979.** Rb-Sr systematics and crustal contamination models for calc-alkaline igneous rocks. *Earth and Planetary Science Letters*, **43**: 385–396.
- Cox, K.G., Bell, J.D., Pankhurst, R.J., 1979.** The Interpretation of Igneous Rocks. George, Allen and Unwin, London.
- Demirbilek, M., Mutlu, H., Fallick, A.E., Sarıöz, K., Kibici, Y., 2018.** Petrogenetic evolution of the Eocene granitoids in eastern part of the Tavşanlı Zone in northwestern Anatolia, Turkey. *Lithos*, **314–315**: 236–259.
- Didier, J., Barbarin, B., 1991.** Enclaves and granite petrology. *Developments in Petrology*, **13**.
- Dilek, Y., Altunkaynak, S., 2009.** Geochemical and temporal evolution of Cenozoic magmatism in western Turkey: mantle response to collision, slab breakoff, and lithospheric tearing in an orogenic belt. *Geological Society Special Publications*, **311**: 213–233.
- Edwards, A., Menzies, M., Thirlwall, M., 1991.** Evidence from Muriah, Indonesia, for the interplay of supra-subduction zone and intraplate processes in the genesis of potassic alkaline magmas. *Journal of Petrology*, **32**: 555–592.
- Elmas, A., Koralay, E., Duru, O., Schmidt, A., 2016.** Geochronology, geochemistry, and tectonic setting of the Oligocene magmatic rocks (Marmaros magmatic assemblage) in Gökçeada Island, northwest Turkey. *International Geology Review*, **59**: 420–447.
- Ersoy, E.Y., Palmer, M.R., 2013.** Eocene-Quaternary magmatic activity in the Aegean: implications for mantle metasomatism and magma genesis in an evolving orogeny. *Lithos*, **180–181**: 5–24.
- Evensen, N.M., Hamilton, P.J., O’Nions, R.K., 1978.** Rare earth abundances in chondritic meteorites. *Geochimica et Cosmochimica Acta*, **42**: 1199–1212.
- Eyuboglu, E., Chung, S.L., Santosh, M., Dudas, F.O., Akaryali, E., 2011.** Transition from shoshonitic to adakitic magmatism in the eastern Pontides, NE Turkey: implications for slab window melting. *Gondwana Research*, **19**: 413–429.
- Faure, G., 1986.** Principles of Isotope Geology. John Wiley and Sons Inc., Canada.
- Gautier, Y., 1984.** Déformations et métamorphismes associés à la fermeture téthysienne en Anatolie Centrale (Région de Sivrihisar, Turquie). Ph.D. Thesis, University Paris.
- Genç, C.Ş., 1998.** Evolution of the Bayramiç magmatic complex. *Journal of Volcanology and Geothermal Research*, **85**: 233–249.
- Göçmengil, G., Karacık, Z., Genç, C.Ş., Prelevic, D., Billor, Z., 2019.** ^{40}Ar - ^{39}Ar ages and petrogenesis of middle Eocene post-collisional volcanic rocks along the Izmir-Ankara-Erzincan suture zone, NE Turkey. *Journal of Asian Earth Sciences*, **173**: 121–142.
- Güleç, N., 1991.** Crust-mantle interaction in western Turkey: implications from Sr and Nd isotope geochemistry of Tertiary and Quaternary volcanics. *Geological Magazine*, **128**: 417–435.
- Güllü, B., 2012.** Temporal and spatial relations of Topkaya and Karakaya (Eskişehir) granitoids. Ph.D. Thesis, Ankara University.
- Güllü, B., Kadioğlu, Y.K., 2012.** Nature of tourmaline bearing quartz veins: Karakaya (Kaymaz) Intrusive Body, Eskişehir, Turkey (in Turkish with English summary). *Yüzüncü Yıl University Journal of The Institute of Natural and Applied Sciences*, **17**: 20–28.
- Güllü, B., Kadioğlu, Y.K., 2017.** Use of tourmaline as a potential petrogenetic indicator in the determination of host magma: CRS, XRD and PED-XRF Methods. *Spectrochimica Acta Part A*, **183**: 68–74.
- Gülmez, F., Genç, C.Ş., Keskin, M., Tüysüz, O., 2013.** A post-collision slab breakoff model for the origin of the Middle Eocene magmatic rocks of the Armutlu–Almacık Belt, NW Turkey and its regional implications. *Geological Society Special Publications*, **372**: 107–139.
- Harris, N.B.W., Pearce, J.A., Tindle, A.G., 1986.** Geochemical characteristics of collision-zone magmatism. *Geological Society Special Publications*, **19**: 67–81.
- Harris, N.B.W., Kelley, S., Okay, A.I., 1994.** Post-collisional magmatism and tectonics in northwest Anatolia. *Contributions to Mineralogy and Petrology*, **117**: 241–252.
- Harrison, T.M., Watson, E.B., 1984.** The behavior of apatite during crustal anatexis: equilibrium and kinetic considerations. *Geochimica et Cosmochimica Acta*, **48**: 1468–1477.
- He, S., Li, Z., Jehani, A.A., Guo, D., Harbi, Z., Zhang, Y., 2021.** Nb-Ta behaviour during magma-to-pegmatite transformation process: record from zircon megacrysts in pegmatite. *Minerals*, **11**: 1139.
- Hibbard, M.J., 1991.** Textural anatomy of twelve magma-mixed granitoid systems. *Developments in Petrology*, **13**: 431–444.
- Irvine, T.N., Baragar, W.R.A., 1971.** A guide to the chemical classification of the common volcanic rocks. *Canadian Journal of Earth Sciences*, **8**: 523–548.
- İlbeyli, N., Kibici, Y., 2009.** Collision-related granite magma genesis, potential sources and tectono-magmatic evolution: comparison between central, northwestern and western Anatolia (Turkey). *International Geology Review*, **51**: 252–278.
- Jacobsen, S.B., Wasserburg, G.J., 1980.** Sm-Nd isotopic systematics of chondrites and achondrites. *Meteoritics*, **15**: 307–308.
- Janasi, V.A., Montanheiro, T.J., Freitas, V.A., Reis, P.M., Negri, F.A., Dantas, F.A., 2007.** Geology, petrography and geochemistry of the acid volcanism of the Paraná Magmatic Province in the Piraju-Ourinhos region, SE Brazil. *Revista Brasileira de Geociências*, **37**: 745–759.
- Johnston, B., 2001.** Magmatic enclaves and evidence for magma mixing in the OAK point granite, Deer Isle, Maine, USA. MSc. Thesis, The University of Maine.
- Karacık, Z., Yılmaz, Y., Pearce, J.A., Ece, O.I., 2008.** Petrochemistry of the south Marmara granitoids, northwest Anatolia, Turkey. *International Journal of Earth Sciences*, **97**: 1181–1200.
- Karslı, O., Dokuz, A., Uysal, I., Aydın, F., Kandemir, R., Wijbrans, J., 2010.** Generation of the Early Cenozoic adakitic volcanism by partial melting of mafic lower crust, Eastern Turkey: implications for crustal thickening to delamination. *Lithos*, **114**: 109–120.
- Karslı, O., Dokuz, A., Aydın, F., Uysal, İ., Tengin, F., Kandemir, R., Santos, J.F., Andersen, T., 2020.** Tracking the timing of Neotethyan oceanic slab break-off: geochronology and geochemistry of the quartz diorite porphyries, NE Turkey. *Journal of Asian Earth Science*, **200**: 104456.
- Kasapoğlu, B., Ersoy, Y.E., Uysal, İ., Palmer, M.R., Zack, T., Koralay, E.O., Karlsson, A., 2016.** The petrology of Paleogene volcanism in the Central Sakarya, Nallihan Region: implications for the initiation and evolution of post-collisional, slab break-off-related magmatic activity. *Lithos*, **246**: 81–98.
- Kaygusuz, A., Arslan, M., Siebel, W., Şen, C., 2011.** Geochemical and Sr–Nd isotopic characteristics of post-collisional calc-alkaline volcanics in the Eastern Pontides (NE Turkey). *Turkish Journal of Earth Sciences*, **20**: 137–159.

- Keskin, M., 2002.** FC-Modeler: a Microsoft Excel spreadsheet program for modeling Rayleigh fractionation vectors in closed magmatic systems. *Computer and Geosciences*, **28**: 919–928.
- Keskin, M., Genç, S.C., Tüysüz, O., 2008.** Petrology and geochemistry of post-collisional Middle Eocene volcanic units in North-Central Turkey: evidence for magma generation by slab breakoff following the closure of the Northern Neotethys Ocean. *Lithos*, **104**: 267–305.
- Koralay, T., Deniz, K., Duman, B., Kadioğlu, Y.K., 2021.** Mineralogical and geochemical characterization and implications for provenance of Roman granite columns in ancient Tripolis (Denizli, Turkey). *Arabian Journal of Geosciences*, **14**: 420.
- Köprübaşı, N., Aldanmaz, E., 2004.** Geochemical constraints on the petrogenesis of Cenozoic I-type granitoids in northwest Anatolia, Turkey: evidence for magma generation by lithospheric delamination in a post-collisional setting. *International Geology Review*, **46**: 705–729.
- Krmíček, L., Cempírek, J., Havlín, A., Přichystal, A., Houzar, S., Krmíčková, M., Gadas, P., 2011.** Mineralogy and petrogenesis of a Ba–Ti–Zr-rich peralkaline dyke from Šebkovice (Czech Republic): recognition of the most lamproitic Variscan intrusion. *Lithos*, **121**: 74–86.
- Maniar, P.D., Piccoli, P.M., 1989.** Tectonic discrimination of granitoids. *GSA Bulletin*, **101**: 635–643.
- Mason, B., Moore, C.B., 1966.** Principles of Geochemistry. John Wiley and Sons, New York.
- Middlemost, E.A.K., 1975.** The basalt clan. *Earth-Science Reviews*, **11**: 337–364.
- Miller, C.F., McDowell, S.M., Mapes, R.W., 2003.** Hot and cold granite? Implications of zircon saturation temperatures and preservation of inheritance. *Geology*, **31**: 529–532.
- Nelson, S.A., 2003.** Magmatic differentiation lecture note. <http://www.tulane.edu/~sanelson/geol212/magmadiff>
- Okay, A.I., 1984a.** The geology of the Ağvanis metamorphic rocks and neighbouring formations. *Bulletin of the Mineral Research and Exploration*, **99**: 16–36.
- Okay, A.I., 1984b.** Distribution and characteristics of the northwest Turkish blueschists. *Geological Society Special Publications*, **17**: 455–466.
- Okay, A.I., 2002.** Jadeite-chloritoid-glaucophane-lawsonite schists from northwest Turkey: unusually high P/T ratios in continental crust. *Journal of Metamorphic Geology*, **20**: 757–768.
- Okay, A.I., 2011.** Tavşanlı Zone: the northern subducted margin of the Anatolide-Tauride Block. *Bulletin of the Mineral Research and Exploration*, **142**: 191–221.
- Okay, A.I., Göncüoğlu, M.C., 2004.** Karakaya Complex: a review of data and concepts. *Turkish Journal of Earth Sciences*, **13**: 77–95.
- Okay, A.I., Satır, M., 2006.** Geochronology of Eocene plutonism and metamorphism in northwest Turkey: evidence for a possible magmatic arc. *Geodinamica Acta*, **19**: 251–266.
- Okay, A.I., Tüysüz, O., 1999.** Tethyan sutures of northern Turkey. *Geological Society Special Publications*, **156**: 475–515.
- Okay, A.I., Satır, M., Shang, C.K., 2008.** Ordovician metagranitoid from the Anatolide-Tauride Block, northwest Turkey-geodynamic implications. *Terra Nova*, **20**: 280–288.
- Okay, A.I., Tüysüz, O., Satır, M., Özkan-Altıner, S., Altıner, D., Sherlock, S., Eren, R.H., 2006.** Cretaceous and Triassic subduction-accretion, HP/LT metamorphism and continental growth in the Central Pontides, Turkey. *GSA Bulletin*, **118**: 1247–1269.
- Özyurt, M., Altunkaynak, Ş., 2020.** Origin of Eocene adakitic magmatism in northwest Turkey. *Journal of Asian Earth Sciences*, **190**: 104147.
- Pearce, J.A., 1983.** Role of the sub-continental lithosphere in magma genesis at active continental margins. In: *Continental Basalt and Mantle Xenoliths* (eds. C.J. Hawkesworth and M.J. Norry): 230–249. Shiva Publishing Ltd., Cheshire.
- Pearce, J.A., 1996.** Sources and setting of granitic rocks. *Episodes*, **19**: 120–125.
- Pearce, J.A., Cann, J.R., 1973.** Tectonic setting of basic volcanic rocks determined using trace element analyses. *Earth and Planetary Science Letters*, **19**: 290–300.
- Pearce, J.A., Harris, N.B.W., Tindle, A.G., 1984.** Trace element discrimination diagrams for the tectonic interpretation of granitic rocks. *Journal of Petrology*, **25**: 956–983.
- Pearce, J.A., Stern, R.J., Bloomer, S.H., Fryer, P., 2005.** Geochemical mapping of the Mariana Arc–Basin system: implications for the nature and distribution of subduction components. *Geochemistry, Geophysics, Geosystems*, **6**: 1–27.
- Rickwood, P.C., 1989.** Boundary lines within petrologic diagrams which use oxides of major and minor elements. *Lithos*, **22**: 247–263.
- Russ, G.P., Burnett, D.S., Lingenfelter, R.E., Wasserburg, G.J., 1971.** Neutron capture on ¹⁴⁹Sm in lunar samples. *Earth and Planetary Science Letters*, **13**: 53–60.
- Schmidt, M.W., 1992.** Amphibole composition in tonalite as a function of pressure: an experimental calibration of the Al-in amphibole barometer. *Contributions to Mineralogy and Petrology*, **110**: 304–310.
- Sha, L.K., 1995.** Genesis of zoned hydrous ultramafic/mafic-silicic intrusive complexes: an MHFC hypothesis. *Earth-Science Reviews*, **39**: 59–90.
- Shand, S.J., 1943.** The Eruptive Rocks. John Wiley, New York.
- Shellnutt, J.G., Jahn, B.M., Zhou, M.F., 2011.** Crustally-derived granites in the Panzhihua region, SW China: implications for felsic magmatism in the Emeishan large igneous province. *Lithos*, **123**: 145–157.
- Shin, T.A., Catlos, E.J., Jacob, L., Black, K., 2013.** Relationships between very high pressure subduction complex assemblages and intrusive granitoids in the Tavşanlı Zone, Sivrihisar Massif, central Anatolia. *Tectonophysics*, **595–596**: 183–197.
- Slaby, E., Martin, H., 2008.** Mafic and felsic magma interaction in granites: the Hercynian Karkonosze Pluton (Sudetes, Bohemian Massif). *Journal of Petrology*, **49**: 353–391.
- Sunal, G., Erturaç, M.K., Topuz, G., Okay, A.I., Sack, T., 2019.** The Early Eocene Ekmekçi granodiorite porphyry in the Karacabey region (Sakarya Zone, NW Turkey). *Turkish Journal of Earth Sciences*, **28**: 589–602.
- Teğör, A.M.C., Yılmaz, Y., 1981.** Tethyan evolution of Turkey: a plate tectonic approach. *Tectonophysics*, **75**: 181–241.
- Wapstra, A.H., Bos, K., 1977.** The 1977 atomic mass evaluation: in four parts part I. Atomic mass table. *Atomic Data and Nuclear Data Tables*, **19**: 177–214.
- Wasserburg, G.J., Jacobsen, S.B., De Paolo, D.J., Mc Culloch, M.T., Wen, T., 1981.** Precise determination of Sm/Nd ratios, Sm and Nd isotopic abundances in standard solutions. *Geochimica et Cosmochimica Acta*, **45**: 2311–2323.
- Watson, E.B., Harrison, T.M., 1983.** Zircon saturation revisited: temperature and composition effects in a variety of crustal magma types. *Earth and Planetary Science Letters*, **64**: 295–304.
- Whitney, D.L., Evans, B.W., 2010.** Abbreviations for names of rock-forming minerals. *American Mineralogist*, **95**: 185–187.
- Whitney, D.L., Teyssier, C., Toraman, E., Seaton, N.C.A., Fayon, A.K., 2011.** Metamorphic and tectonic evolution of a structurally continuous blueschist-to-Barrovian terrane, Sivrihisar Massif, Turkey. *Journal of Metamorphic Geology*, **29**: 193–211752.
- Wilson, M., Bianchini, G., 1999.** Tertiary-Quaternary magmatism within the Mediterranean and surrounding regions. *Geological Society Special Publications*, **156**: 141–168.
- Yılmaz, Y., 1981.** Tectonic evolution of the southern margin of the Sakarya continent, NW Turkey (in Turkish with English summary). *Istanbul Earth Sciences Review*, **1**: 33–51.
- Zindler, A., Hart, S.R., 1986.** Chemical geodynamics. *Annual Review of Earth and Planetary Sciences*, **14**: 493–571.
- Zheng, Y.C., Hou, Z.Q., Fu, Q., Zhu, D.C., Liang, W., Xu, P., 2016.** Mantle inputs to Himalayan anatexis: insights from petrogenesis of the Miocene Langkazi leucogranite and its dioritic enclaves. *Lithos*, **264**: 125–140.
- Zoroğlu, O., 2009.** Geology, petrology and origin of enclaves of Sivrihisar-Günyüzü (Eskişehir) granitoids. Ph.D. Thesis, Ankara University.

APPENDIX 2 The argon release values of the samples according to $^{40}\text{Ar}/^{39}\text{Ar}$ step-heating

Temp. (°C)	$^{40}\text{Ar}/^{39}\text{Ar}$	$^{37}\text{Ar}/^{39}\text{Ar}$	$^{36}\text{Ar}/^{39}\text{Ar}$	$^{40}\text{Ar}^*/^{39}\text{Ar}_k$	$^{40}\text{Ar}^*$ (%)	$^{39}\text{Ar}_k$ (%)	Age \pm 2s (Ma)
T-129 Bio weight=5.4mg							
650 °C	195.00646	0.13978	0.61693	12.719315	6.52	0.26	53.84 \pm 30.41
700 °C	431.05235	0.02855	1.42429	10.176396	2.36	1.04	43.20 \pm 70.13
750 °C	93.68346	0.01046	0.28153	10.490732	11.20	3.74	44.52 \pm 13.86
790 °C	12.66620	0.00716	0.00801	10.299199	81.31	4.76	43.72 \pm .74
830 °C	12.01506	0.00657	0.00571	10.328945	85.97	5.44	43.84 \pm .60
870 °C	12.05556	0.00481	0.00502	10.571880	87.69	4.98	44.86 \pm .60
910 °C	11.68889	0.00479	0.00426	10.431266	89.24	6.47	44.27 \pm .57
950 °C	11.96374	0.00707	0.00490	10.515058	87.89	7.22	44.62 \pm .58
980 °C	11.75665	0.00843	0.00402	10.569389	89.90	7.21	44.85 \pm .55
1010 °C	11.10006	0.00627	0.00242	10.385651	93.56	8.53	44.08 \pm .50
1040 °C	10.84941	0.00756	0.00140	10.437786	96.21	11.60	44.30 \pm .46
1070 °C	10.77984	0.00639	0.00115	10.440028	96.85	12.93	44.31 \pm .46
1100 °C	10.74702	0.00580	0.00104	10.439543	97.14	13.07	44.31 \pm .47
1130 °C	10.70008	0.00661	0.00112	10.368614	96.90	10.33	44.01 \pm .46
1160 °C	12.05440	0.03598	0.00550	10.431316	86.53	1.69	44.27 \pm 2.04
1310 °C	22.18160	0.10555	0.03852	10.810586	48.73	0.65	45.86 \pm 2.30
1400 °C	116.64498	0.28992	0.30964	25.182268	21.58	0.07	105.08 \pm 39.88
T-YK. (1)46 Hbl weight=7.4mg							
850 °C	237.90049	1.35428	0.73451	20.982942	8.81	1.51	87.73 \pm 48.51
950 °C	282.23281	5.27585	0.92478	9.421014	3.32	1.43	39.91 \pm 49.87
1000 °C	122.16787	10.02720	0.38962	7.901459	6.41	1.77	33.54 \pm 22.19
1020 °C	36.60272	8.44221	0.08796	11.367267	30.83	2.93	48.05 \pm 5.46
1040 °C	15.94268	11.01245	0.02102	10.711546	66.56	16.72	45.31 \pm 1.35
1050 °C	13.00299	10.86477	0.01197	10.430257	79.47	32.02	44.14 \pm .87
1060 °C	12.30257	10.71083	0.01009	10.270608	82.72	24.60	43.47 \pm .88
1070 °C	17.03755	6.61056	0.02040	11.604524	67.73	3.00	49.04 \pm 2.84
1110 °C	26.91443	14.31873	0.05047	13.304596	48.83	1.26	56.12 \pm 6.13
1140 °C	19.71088	12.25152	0.02636	13.035809	65.44	3.35	55.00 \pm 2.87
1170 °C	19.34970	13.65632	0.03014	11.669765	59.61	4.00	49.31 \pm 2.87
1200 °C	18.54805	13.36812	0.03122	10.511988	56.03	4.50	44.48 \pm 2.47
1260 °C	31.26069	17.09813	0.06211	14.487137	45.67	1.11	61.02 \pm 7.10
1290 °C	28.78991	16.22877	0.05895	12.843558	43.99	1.38	54.20 \pm 5.92
1350 °C	49.08700	18.40130	0.11546	16.710463	33.51	0.43	70.21 \pm 18.16
K-120 Bio weight=5.8mg							
650 °C	69.91473	0.03776	0.18428	15.462684	22.12	0.62	66.36 \pm 10.00
730 °C	141.59322	0.01123	0.43044	14.398283	10.17	2.21	61.87 \pm 21.34
770 °C	22.16321	0.00631	0.02272	15.449079	69.71	1.74	66.30 \pm 1.64
810 °C	15.90924	0.01224	0.00871	13.335243	83.82	3.52	57.37 \pm .92
850 °C	14.61026	0.00178	0.00707	12.520506	85.70	5.72	53.92 \pm .93
890 °C	14.56484	0.00157	0.00478	13.152495	90.30	7.66	56.60 \pm .66
920 °C	14.79198	0.01240	0.00380	13.670653	92.42	7.31	58.79 \pm .80
950 °C	14.75457	0.00026	0.00333	13.770868	93.33	8.70	59.21 \pm .65
980 °C	14.57406	0.00000	0.00428	13.308359	91.32	14.73	57.26 \pm .62
1010 °C	14.71118	0.00007	0.00345	13.692105	93.07	19.19	58.88 \pm .64
1040 °C	15.15922	0.01809	0.00715	13.046646	86.06	11.58	56.15 \pm .72
1070 °C	16.08245	0.01461	0.00436	14.794989	91.99	6.38	63.54 \pm .71
1110 °C	16.70203	0.01522	0.00278	15.880681	95.08	5.46	68.12 \pm .81
1150 °C	17.66774	0.00000	0.01124	14.344290	81.19	3.24	61.64 \pm 1.57
1190 °C	19.68375	0.00000	0.01936	13.960890	70.93	1.08	60.02 \pm 4.08
1230 °C	23.53029	0.00523	0.04141	11.295265	48.00	0.41	48.71 \pm 4.71
1330 °C	26.05049	0.05932	0.05763	9.025809	34.65	0.47	39.03 \pm 9.47